

CORONAL STRUCTURE AND ABUNDANCES OF CAPELLA FROM SIMULTANEOUS *EUVE* AND *ASCA* SPECTROSCOPY

N. S. BRICKHOUSE, A. K. DUPREE, AND R. J. EDGAR

Smithsonian Astrophysical Observatory, 60 Garden Street, Cambridge, MA 02138; nbrickhouse@cfa.harvard.edu

D. A. LIEDAHL

Lawrence Livermore National Laboratory, P.O. Box 808, L-41, Livermore, CA 94550

S. A. DRAKE AND N. E. WHITE

Laboratory for High Energy Astrophysics, Code 668, NASA/Goddard Space Flight Center, Greenbelt, MD 20771

AND

K. P. SINGH

Department of Astronomy & Astrophysics, Tata Institute of Fundamental Research, Homi Bhabha Road, Mumbai 400 005, India

Received 1999 June 11; accepted 1999 September 29

ABSTRACT

We report analysis of the simultaneous 1996 March *EUVE* and *ASCA* observations of the spectroscopic binary Capella. The *EUVE* spectrum is dominated by lines of highly ionized Fe, requiring a continuous emission-measure distribution over a wide range of temperatures. The *ASCA* spectrum shows He-like line emission features of S, Si, and Mg, as well as unresolved L-shell emission lines of Fe and Ni and H-like and He-like Ne lines. The flux in these line features cannot be determined independently from the continuum flux. The *ASCA* spectrum is relatively soft, with few counts above 4 keV. The emission-measure distribution determined by Line-Based Analysis of the EUV Fe line intensities is well constrained from $T_e \sim 6 \times 10^5$ to 2×10^7 K, but it is not constrained above this range since Fe XXIV is the highest temperature line observed with *EUVE*. Since repeated observations of Capella by *EUVE* have shown that emission-line intensities of the hottest EUV-emitting material (Fe XXI to XXIV) vary by factors up to 4, the *ASCA* spectrum is important for extending the temperature coverage. Thus, the high-energy cut-off of the *ASCA* spectrum provides a constraint on the highest temperature emission measures. In principle, elemental abundances are determined from global fits to the *ASCA* spectrum; however, no well-fitting model has been found for the high signal-to-noise *ASCA* performance verification spectrum of Capella (1993 September 2). The newer *ASCA* spectrum of Capella (1996 March 3–4) shows a similar pattern of fitting difficulties. Using the *EUVE* measurements (1996 March 3–7) to constrain models, we have conducted sensitivity studies of the atomic data, source physics, and instrument calibration. The plasma spectral emission models (Raymond-Smith, MEKAL, SPEX) around 1.2 keV appear to have flux deficits relative to the observed *ASCA* count spectrum. New atomic models by Liedahl and Brickhouse, calculated with the HULLAC code, provide a set of lines—missing from the existing plasma codes—to fill in this flux deficit. Incorporating these additional lines dramatically improves the spectral model fits to the data, allowing reliable determination of elemental abundances. The successful application of the new atomic models to the Capella problem can have widespread implications, affecting spectral models of galaxies, cluster cooling flows, and supernova remnants, as well as other stellar coronae. Analysis with the new atomic models of the simultaneous *ASCA* and *EUVE* data confirms the previous *EUVE* results that the continuous emission-measure distribution of Capella has a strong enhancement at $T_e \sim 6 \times 10^6$ K. While a two-temperature model actually provides a better fit to the *ASCA* spectrum than the *EUVE*-derived continuous model, the *EUVE* data are not well fitted with only two temperatures. We find that the abundances of Mg, Si, S, and Fe are consistent with solar photospheric values, while Ne appears to be underabundant by a factor of ~ 3 to 4.

Subject headings: binaries: spectroscopic — stars: abundances — stars: coronae — stars: individual (Capella) — ultraviolet: stars — X-rays: stars

1. INTRODUCTION

Studies of the coronal structure and abundances of cool stars seek to characterize the relationship between stellar activity and rotation, atmospheric heating, and energy transport. Spectral diagnostics provide measurements of the physical conditions of the stellar corona—electron temperature, density, and elemental abundances. The binary system Capella (α Aur; HR 1708; HD 34029) has a rich, high-energy emission-line spectrum intermediate in energy between slowly rotating, solar-type single stars such as α Centauri and Procyon and the shorter period, X-ray luminous RS CVn binary systems, such as HR 1099.

At a distance of 12.94 ± 0.15 pc (Perryman et al. 1997), Capella is one of the brightest stellar X-ray sources. Early X-ray observations of Capella excluded the possibility of a gravitationally bound corona, requiring instead that the hot plasma be magnetically confined (Catura, Acton, & Johnson 1975). Composed of a G8 III or K0 III star plus a G1 III star in a 104 day orbit, the G1 giant, located in the Hertzsprung gap, rotates rapidly with an ~ 8 day period (Hummel et al. 1994; Strassmeier & Fekel 1990). The two stars are believed to contribute roughly equally to the X-ray emission (Ayres, Schiffer, & Linsky 1983; Linsky et al. 1998), which complicates any interpretation of the compos-

ite spectrum in terms of individual stellar properties. Comparing the Capella spectrum to spectra of the prototypical single stars β Ceti (K0 III) and 31 Comae (G0 III) provides insight into the likely contributions from the two Capella components (see Ayres et al. 1998).

This introduction summarizes previous studies of the coronal structure and abundances of the Capella system, discusses problems with the 1993 *ASCA* spectral analysis, and motivates the 1996 simultaneous *EUVE* and *ASCA* campaign. Section 2 presents the observations and standard individual data analyses, while § 3 describes the joint analysis. Model uncertainties and improvements are summarized in § 4, leading to the presentation in § 5 of the application of improved models to the joint analysis. In § 6, we consider the physical implications of our results, and in § 7 we present the conclusions as to the coronal structure and abundances of Capella.

1.1. Studies of the Coronal Structure of Capella

Holt et al. (1979) first demonstrated, in their analysis of spectra obtained with the Solid State Spectrometer (SSS) on *Einstein*, that the coronal structure of Capella is inconsistent with an isothermal plasma. Swank et al. (1981), also with SSS data, and Mewe et al. (1982), using observations obtained with the Objective Grating Spectrometer on *Einstein*, confirmed that at least two temperature components were needed to obtain an acceptable fit to the spectra.

The Focal Plane Crystal Spectrometer (FPCS) on *Einstein* detected individual X-ray lines of O VIII, Fe XVII, and Fe XX, which could be modeled by a simple distribution of plasma temperatures suggestive of magnetic loop structures (Vedder & Canizares 1983). The Capella spectrum obtained with the Transmission Grating Spectrometer on *EXOSAT*, with approximately 3 Å resolution from 10 to 200 Å, allows the identification of several additional prominent lines while generally confirming the dominance of two-temperature components (Lemen et al. 1989).

During the performance verification and in-flight calibration phases of both the *EUVE* and *ASCA* missions, high-quality EUV and X-ray spectra of Capella were obtained. The range of ionization states of Fe in the *EUVE* spectrum of 1992 December 10–13 demonstrated for the first time that the high-temperature emission-measure (EM) distribution of Capella is a continuous, though not “smooth,” function of the electron temperature T_e (Dupree et al. 1993). The EM distribution is characterized by a minimum near $T_e \sim 10^6$ K (where the solar EM distribution peaks), a characteristic enhancement or “bump” at $T_e \sim 6 \times 10^6$ K, and evidence for emission at $T_e > 10^7$ K.

While the physical interpretation of EM distribution bumps remains unclear, Dupree (1996) has suggested that narrow bumps in the high-temperature EM distribution might be properties of rapidly rotating stars. Brickhouse & Dupree (1998) present both spectroscopic and light curve evidence for the W UMa source 44i Boo, suggesting that its EM distribution bump derives from a high-latitude, high magnetic field (~ 1 kG) region. Density diagnostics for Capella at temperatures associated with the EM distribution bump also suggest high density ($N_e \sim 10^{12}$ cm $^{-3}$; Dupree et al. 1993; Brickhouse 1996). Griffiths & Jordan (1998) find EM distribution bumps in three RS CVn systems (AR Lac, HR 1099, and II Peg). They argue that the density-sensitive resonance line Fe XXI λ 128.7 requires a lower density (by up to an order of magnitude) from EM

distribution fitting than is derived from line-ratio diagnostics. Adopting this lower density value still requires thermal pressures greater than 10^{18} cm $^{-3}$ K, i.e., 2 orders of magnitude larger than those of solar active regions. High densities and steep EM distributions have important consequences within the framework of quasi-static loop models as well, such as requiring the expansion of loop cross section with height and the addition of more loop populations (Schrijver, Lemen, & Mewe 1989; van den Oord et al. 1997).

Recently *Beppo-SAX*/LECS observations of Capella have been successfully modeled with two temperatures; however, the model does not agree well with (nonsimultaneous) *EUVE* data (Favata et al. 1997). For the LECS data, the best-fit two-temperature MEKAL model gives $\log [T_1 \text{ (K)}] = 6.88$ (6.85, 6.92) and $\log [EM_1 \text{ (cm}^{-3}\text{)}] = 52.79$ (52.71, 52.86) and $\log [T_2 \text{ (K)}] = 7.08$ (6.99, 7.16) and $\log [EM_2 \text{ (cm}^{-3}\text{)}] = 52.20$ (51.62, 52.44), normalizing the EM values to the *Hipparcos* distance given by Perryman et al. (1997).

1.2. Studies of the Coronal Abundances of Capella

The study of coronal abundance patterns in cool stars has emerged parallel to EM distribution studies as a possible approach to understanding heating and diffusion, though the physical mechanisms by which coronal abundances diverge from photospheric abundances are not understood as yet (see Drake, Laming, & Widing 1997 and references therein). Despite controversy on the details of specific observational evidence, there is a growing consensus (see Jordan et al. 1998) on the following points.

1. Solar coronal abundance patterns vary depending on the type of coronal region (e.g., Sheeley 1996). Values appropriate to the photosphere are found, as well as values associated with the first ionization potential (FIP) effect, in which low FIP elements are enhanced relative to high FIP elements.
2. Evidence from *EUVE* stellar observations exists for both stellar-photospheric (Drake, Laming, & Widing 1995) and FIP-effect (Drake, Laming, & Widing 1997) coronal abundance patterns.
3. Evidence exists from both *EUVE* and *ASCA* for overall metal abundance depletion (MAD) (Antunes, Nagase, & White 1994; Stern et al. 1995; White et al. 1994; Schmitt et al. 1996).

Photospheric abundances are not well known for Capella; hence, we compare abundances to the commonly used solar photospheric abundances compiled by Anders & Grevesse (1989, hereafter AG89). Using high-resolution spectroscopy and photometric catalogs, McWilliam (1990) derives the stellar atmosphere parameters and abundances for a sample of 671 G and K field giants, finding that the photospheric Fe/H abundance ratio of Capella is 0.43 (0.26, 0.71) times the AG89 ratio. This value presumably reflects the more slowly rotating late-G star. Randich, Giampapa, & Pallavicini (1994) find the late and early G stars to have Fe/H ratios of 0.4 and 1.1 times the AG89 value, respectively. [Their value $\log N(\text{Fe}) = 7.63$ has been converted to the AG89 value $\log N(\text{Fe}) = 7.67$, with $\log N(\text{H}) = 12.00$.] Pilachowski & Sowell (1992) also find good agreement for both Capella components with the solar value for Ca. On the other hand, if Capella is an outlying member of the Hyades cluster, its Fe/H abundance ratio would be about twice solar (see Eggen 1960; Ayres 1988). We note that the

newer solar Fe/H abundance ratio of Grevesse, Noels, & Sauval (1992) is somewhat lower than that of AG89 (log $N(\text{Fe}) = 7.53$).

Drake et al. (1994) have reanalyzed the SSS data observations of Capella using a two-temperature (2-T) model with variable abundances, finding ~ 0.5 – 1.0 times AG89 abundances for Mg, Si, S, and Fe but well below the AG89 values for O and Ne. The SAX model gives a global metal abundance of 0.68 ± 0.05 times the AG89 value.

Either possible scenario—that the stellar coronal abundance is anomalous relative to the photospheric abundances or that the photospheric abundances themselves are anomalous—raises interesting questions. For the former scenario, a mechanism must be found to explain differences among elements in transport or diffusion from the photosphere to the corona for either a FIP or MAD effect. While magnetic fields presumably play a preferential role for charged ions relative to neutrals, and gravitational effects are mass-dependent, no model currently explains solar or stellar coronal abundance patterns. Alternatively, the depletion of metals in stellar photospheres is also problematic. Evidence for this possibility has existed for RS CVn binaries for some time (Naftilan & Drake 1977) and has held up in later studies (Randich, Gratton, & Pallavicini 1993), but it may be an observational effect (see Ortolani et al. 1997 for a recent discussion).

1.3. Problems with Fitting the 1993 ASCA Capella Spectrum

Because we continue to have problems fitting the 1993 ASCA Capella spectrum, as well as with reconciling it with nonsimultaneous EUVE spectra, we focus on the simultaneous 1996 data for the rest of the analysis in this paper. In this section, we discuss briefly the analysis of the 1993 ASCA spectrum.

The ASCA performance verification (PV) phase spectrum of the spectroscopic binary Capella, obtained 1993 September 2 with 14,442 s exposure, shows a rich spectrum with emission-line features (Fig. 1). Early analysis of the 1993 ASCA spectrum of Capella suggested that its coronal abundances are lower than solar photospheric (AG89) values;

however, the poor fit to the ASCA spectrum ($\chi_{\text{red}}^2 \sim 6$) requires further investigation to determine if the derived abundances are reliable (Drake 1996). Figure 1 shows the 1993 SIS0 spectrum with the “best” 2-T model. As pointed out by Drake, Singh, & White (1996), the MEKAL 2-T model gives a poor fit to the Capella spectrum at 10 \AA (1.2 keV).

Since the 1 keV X-ray spectrum is produced by plasma at the same temperatures as the EUV Fe lines, we expect and find that one of the two temperatures in the 2-T model is consistent with the bump temperature derived from the EUVE spectra (Dupree et al. 1993). We have been unable to improve the fit to the 1993 ASCA spectrum by using the 1992 EUVE data and derived EM distribution model. The EM distribution of Dupree et al. (1993) overpredicts the ASCA highest energy flux by about a factor of 3, showing poor fits to other regions of the X-ray spectrum as well. The overprediction of the highest energy flux is likely caused by both the poor constraint provided by EUVE and time variation of the source. We can find models that are compatible with EUVE data, the peak of the 1993 ASCA count spectrum and the high-energy ASCA cut-off; however, these models still do not provide acceptable fits to the entire ASCA spectrum. In fact, we have not been able to find any continuous-temperature (Cont-T) EM-distribution, variable-abundance models to fit the 1993 ASCA spectrum, even with the improved spectral models presented in § 4.

Short-term EUV and X-ray variability, as measured with the broadband EUVE Deep Survey instrument and with the ASCA SIS detectors, is less than $\pm 30\%$. Optical to UV emission is remarkably constant from year to year (Ayles et al. 1995). On the other hand, monitoring of Capella with EUVE under the Guest Observer Program has found significant long-term variability in the highest temperature emission lines (Dupree & Brickhouse 1996), with some EUV line intensities showing changes from one observation to the next, spanning a three-year period, by factors of 3 to 4. The highest temperature lines ($T_e > 10^7 \text{ K}$) appear to be the most variable, while lines formed at the EM distribution enhancement ($T_e \sim 6 \times 10^6 \text{ K}$) do not change by more than

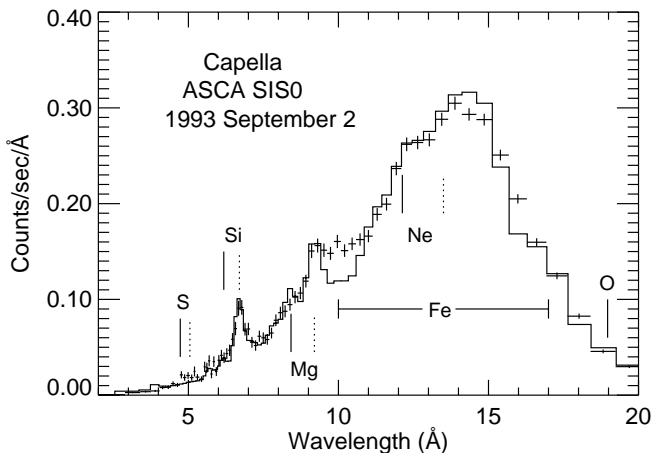


FIG. 1a

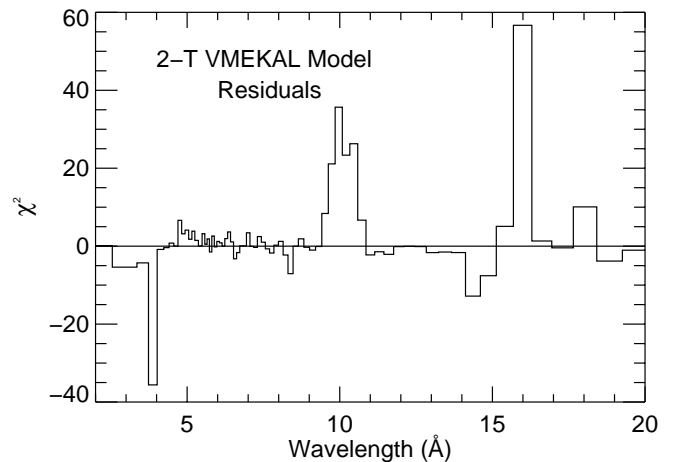


FIG. 1b

FIG. 1.—(a) ASCA PV phase spectrum of Capella obtained 1993 September 2 with SIS0, with “best” fit ($\chi_{\text{red}}^2 = 5.5$) 2-T model and variable abundances (model parameter given in Tables 2 and 3). The VMEKAL model in XSPEC is used. The H-like Ly α line positions of O, Ne, Mg, Si, and S are marked with solid lines, while the strongest He-like lines are marked with dotted lines. In principle, Fe L-shell emission extends over most of the waveband shown, from ~ 6 to 17 \AA ; however, for the Capella spectrum, the strongest emission is between 10 and 17 \AA . (b) χ^2 for each bin calculated as the square of the difference between the observed flux and the model flux divided by the square of the statistical error σ . The value is plotted as positive or negative depending on the sign of the residual.

$\pm 30\%$, and lines formed at temperatures below the enhancement ($T_e \lesssim 4 \times 10^6$ K) change by factors of less than 2. Variability of the highest temperature lines probably explains the low intensity of the Fe xxI UV forbidden line (Linsky et al. 1998) relative to EUV Fe xxI line intensities.

1.4. Overview of the 1996 EUVE and ASCA Capella Observation and Spectral Analysis

With a time-variable coronal source, simultaneous EUVE and ASCA observations provide an opportunity to determine the structure and abundance of its corona, exploiting the complementary features of the two instruments. This paper reports the results of the joint analysis of our 1996 March EUVE and ASCA observations. Within the parameters of standard plasma emission models, we are unable to find any acceptable model fit to the 1996 ASCA spectrum. In order to explore specific systematic errors, we use the EUVE observations to impose constraints and narrow the range of possible models. With a high signal-to-noise ratio (S/N) and good spectral resolution, the Capella EUVE Fe line data provide numerous consistency checks (several lines from each of the dominant ions and branching ratio pairs) and have been thoroughly benchmarked with respect to tokamak data and to theoretical atomic structure models (Brickhouse, Raymond, & Smith 1995). Thus, we are able to assign confidence levels to individual line-intensity measurements as well as to the total EM distribution model.

Throughout our analysis, we use the empirically derived emission-measure (EM) distribution, with $EM = \int N_e N_H dV$, where N_e is the electron density, N_H is the hydrogen density, and the volume integration is performed over some temperature interval. The EM distribution is constructed from discrete temperature interval components. For Cont-T models, the temperature interval used here is fixed at 0.1 dex, whereas for the two-temperature (2-T) models, the temperatures are also fitted, as implemented in XSPEC (Arnaud 1996). We use the EM distribution rather than its derivative, the differential emission measure ($DEM = N_e N_H dV/dT$), in order to facilitate the comparison between our 2-T and Cont-T models, as well as with previously published 2-T models. Generally, EUVE observations require many temperature components in the fit, whereas ASCA observations generally require only one or two.

For our analysis, we construct a hierarchy of spectral features, favoring strong, isolated emission lines of EUVE over broadband spectral fluxes. Unlike Global Fitting Analysis (GFA) of simultaneous ASCA and EUVE observations of cool stars (e.g., Mewe et al. 1996), Line-Based Analysis (LBA) allows modeling uncertainties to be explored on the basis of related spectral features. For example, the X-ray Fe xviii line intensities are directly predicted from the EUV Fe xviii line intensities observed in the EUVE spectrum. In our best-fit model, as described below, lines from Fe xvii, xviii, and xix contribute 77% of the flux in a 1.0 Å bin centered at 14.0 Å, near the peak of the count spectrum. Thus, good agreement between the model and the data in this spectral region would be expected. LBA may prove generally useful for exploring other modeling problems as well.

The puzzling Capella ASCA spectrum has led to the development of more complete plasma models that contain transitions from levels of high n (D. A. Liedahl & N. S. Brick-

house, 1999, in preparation). With these new models, we determine EM distributions and elemental abundances using the best understood and most reliable information from both EUVE and ASCA.

2. OBSERVATIONS AND STANDARD SPECTRAL ANALYSIS

2.1. EUVE Data Reduction and Analysis

Figure 2 shows the 1996 March 3–7 EUVE Short Wavelength (SW) and Medium Wavelength (MW) spectra of Capella. The Long Wavelength (LW) spectrum is not shown. Total exposure times are 120,896, 115,980, and 125,820 s for the SW, MW, and LW spectrometers, respectively. The data have been reduced using version EGOCS 1.6.1 of the EGO software and version EGODATA 1.12 of the reference data set. The extraction, line-intensity measurements, and S/N determination are described in detail in Brickhouse & Dupree (1998). In brief, we have performed optimized extractions from the summed two-dimensional images by removing an averaged background evaluated on either side of the spectrum. For isolated lines, we require that the Gaussian line width be consistent with the instrumental profile and sum over the line profile to obtain total counts. For the SW spectrometer, a small continuum contribution is subtracted from the SW flux, which is determined by visual examination of the lowest flux bins and the relative noise levels. Composite spectra of Capella confirm the apparent continuum level (Brickhouse 1996). Blended lines are treated by standard multiple Gaussian fitting methods.

The EUVE spectrum contains strong lines of highly ionized Fe, which we use to determine the EM distribution over the appropriate temperature range. Lines used to determine the EM distribution are listed in Table 1, with comments detailing assessments of line blending for individual features, as appropriate. The observed line fluxes are corrected for interstellar absorption, assuming a H/He abundance ratio of 11.6 (Kimble et al. 1993). We adopt an interstellar column density of $N_H = 1.8 \times 10^{18} \text{ cm}^{-2}$ (Linsky et al. 1993).

Using the atomic emission-line models of Brickhouse et al. (1995), we determine the EM distribution that is shown in Figure 3. (The high-temperature range has been constrained by the ASCA observation, as described in the next section.) The model EM distribution is adjusted iteratively to obtain reasonable agreement with the EUV lines. Table 1 also lists the S/N, thus showing the high statistical significance of the line intensities. As discussed by Brickhouse et al. (1995), uncertainties in the atomic data are likely to be the dominant sources of error in this analysis. The level of agreement between the predicted and observed line intensities (Fig. 4a) is good and consistent with our understanding of the systematic errors. Within the combined statistical and model error estimates from EUVE, the predicted ASCA spectrum should be well constrained by a small number of model parameters. The effect of the model uncertainties on the X-ray spectral predictions is discussed in detail below.

The EM distribution derived from the strong Fe lines listed in Table 1 can serve to predict other high-temperature lines in the EUV. Lines from the lower temperature plasma of the transition region are not well predicted from the EUV since most of the EUV transition region lines are weak; furthermore, composite EUVE spectra of Capella show that

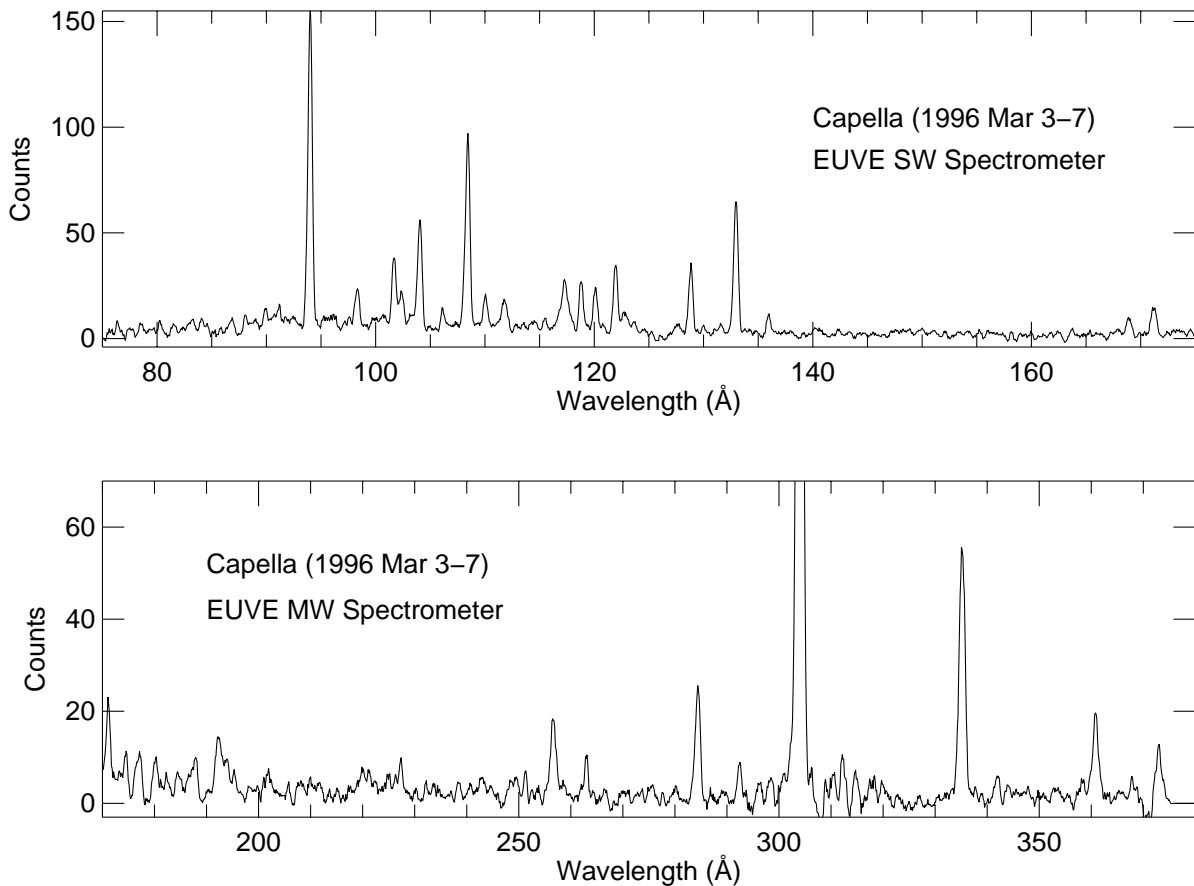


FIG. 2.—*EUVE* spectra of Capella obtained 1996 March 3–7, showing the SW and MW spectrometer data. The exposure times are 120,896 and 115,980 s for the SW and MW spectrometers, respectively. The LW spectrometer (data not shown) exposure time is 125,820 s.

these lines are weaker than their ultraviolet counterparts (Brickhouse, Dupree, & Raymond 1996). He II $\lambda 303.78$ is the exception, but its excitation mechanism is complicated by photoionization, and the line is most likely optically thick.

Since these transition region ions do not contribute to the *ASCA* spectrum, we do not address them in this paper except to note that their presence makes the application of the Global Fitting Analysis (GFA), as performed by Schrijver et al. (1995), far more susceptible to errors from weak lines than our Line-Based Analysis (LBA). Brickhouse (1996) discusses the use of high-temperature lines of elements other than Fe for abundances (see § 6); such lines are significantly weaker than the Fe lines.

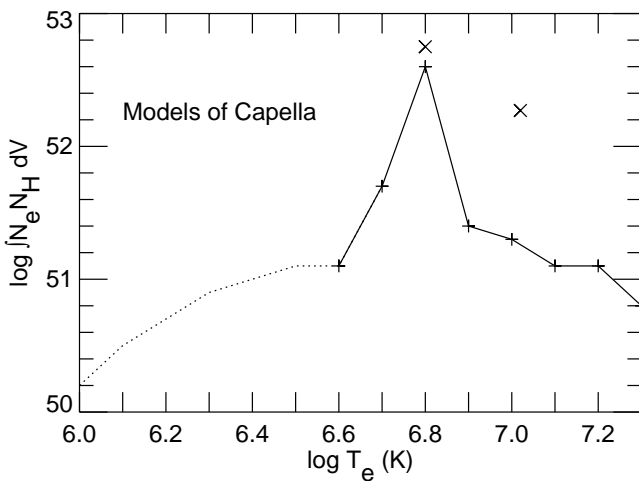


FIG. 3.—EM distribution derived from the EUV Fe line intensities listed in Table 1 for the Capella data of 1996 March 3–7, shown as a solid curve extended to lower temperature by a dotted curve. The model below $\log T_e = 6.6$ (i.e., the dotted curve) does not have a significant effect on fits to the *ASCA* spectrum but is required by the strong Fe IX $\lambda 171.07$ line. Plus signs mark the temperatures used in the continuous-temperature (Cont-T) models, as described in the text. Crosses mark the 2-T model that best fits the *ASCA* SIS0 + SIS1 spectra (see the seventh column of Table 2).

2.2. *ASCA* Data Reduction and Standard Analysis

On 1996 March 3–4 we obtained *ASCA* observations of Capella that also overlapped with the 1996 March 3–7 *EUVE* observations.

Spectra were accumulated in Bright Mode for 21,127 s in SIS0 and for 20,787 s in SIS1. The source regions taken for our analysis have radius 3:1 for SIS1 and 3:8 for SIS0, while the background was taken from source-free regions. The spectral data were grouped so that there were at least 20 counts per pulse-height bin. Since the spectrum is relatively soft, the GIS spectra do not provide additional information, and we will not include their analyses here, except to note that the GIS spectra are consistent with our results.

The standard variable-abundance, thermal models (Raymond-Smith and MEKAL) in XSPEC version 10.0 (see Arnaud 1996) do not provide acceptable fits. Tables 2 and 3 give the “best fit” ($\chi^2_{\text{red}} = 3.15$) model parameters for the 2-T VMEKAL model, with *ASCA* data and model shown in Figure 5. The comparison of abundance determinations

TABLE 1
EUV EMISSION LINES IN CAPELLA SPECTRUM^a

| Ion | λ_{lab} (Å) | λ_{obs} (Å) | Total Counts | S/N | Flux ^b (photons cm ⁻² s ⁻¹) | Flux ^c (photons cm ⁻² s ⁻¹) | Blends and Other Comments |
|--------------------------------|-------------------------------|-------------------------------|--------------|------|--|--|--|
| Short Wavelength Spectrometer | | | | | | | |
| Fe XIX | 91.02 | 91.11 | 87.7 | 8.9 | 3.74e-04 | 3.91e-04 | Fe XXI λ 91.28 |
| Fe XVIII | 93.92 | 94.00 | 1116.0 | 31.6 | 4.59e-03 | 4.81e-03 | |
| Fe XIX | 101.55 | 101.69 | 234.5 | 13.9 | 9.46e-04 | 1.00e-03 | Isolated peak ^d |
| Fe XXI | 102.22 | 102.32 | 123.8 | 9.6 | 4.81e-04 | 5.12e-04 | Complex blend ^d |
| Fe XVIII | 103.94 | 104.03 | 393.3 | 17.4 | 1.55e-03 | 1.65e-03 | |
| Fe XIX | 108.37 | 108.41 | 702.0 | 24.8 | 2.81e-03 | 3.02e-03 | |
| Fe XIX | 109.97 | 110.04 | 125.0 | 9.3 | 5.14e-04 | 5.53e-04 | Fe XX λ 110.63 |
| Fe XIX | 111.70 | 111.77 | 132.5 | 9.8 | 5.62e-04 | 6.07e-04 | |
| Fe XXII | 117.17 | 116.99 | 217.4 | 12.9 | 1.05e-03 | 1.15e-03 | Appears blended, probably with Fe XXI λ 117.51 |
| Fe XX | 118.66 | 118.83 | 191.4 | 10.9 | 9.54e-04 | 1.05e-03 | |
| Fe XIX | 120.00 | 120.11 | 165.6 | 10.2 | 8.56e-04 | 9.41e-04 | |
| Fe XX | 121.83 | 121.96 | 250.8 | 13.5 | 1.38e-03 | 1.52e-03 | |
| Fe XXI | 128.73 | 128.83 | 222.6 | 12.8 | 1.48e-03 | 1.66e-03 | |
| Fe XXIII | 132.85 | 132.96 | 471.0 | 20.1 | 3.61e-03 | 4.08e-03 | Fe XX λ 132.85 |
| Fe XXII | 135.78 | 135.96 | 72.1 | 5.7 | 5.96e-04 | 6.78e-04 | O V λ 135.52 |
| Fe IX | 171.07 | 171.19 | 115.8 | 9.7 | 3.00e-03 | 3.79e-03 | |
| Medium Wavelength Spectrometer | | | | | | | |
| Fe IX | 171.07 | 171.09 | 187.8 | 11.4 | 2.98e-03 | 3.77e-03 | Near filter edge |
| Fe XXIV | 192.04 | 192.30 | 175.9 | 10.2 | 3.33e-03 | 4.47e-03 | Complex blend ^e |
| Fe XV | 284.15 | 284.38 | 230.8 | 12.5 | 5.25e-03 | 1.20e-02 | |
| Fe XVI | 335.41 | 335.18 | 593.6 | 22.0 | 1.10e-02 | 3.81e-02 | |
| Fe XVI | 360.80 | 360.85 | 219.3 | 11.4 | 3.61e-03 | 1.59e-02 | |
| Long Wavelength Spectrometer | | | | | | | |
| Fe XVI | 335.41 | 335.45 | 865.3 | 28.6 | 9.33e-03 | 3.23e-02 | |
| Fe XVI | 360.80 | 359.77 | 604.8 | 20.9 | 6.02e-03 | 2.65e-02 | Appears wide |

^a EUVE observations of 1996 March 3–7. Total integration times are 120,896, 115,980, and 125,820 s for SW, MW, and LW spectrometers, respectively. Data have been reduced using version EGOCS 1.6.1 of the EGO software, and version EGODATA 1.12 of the reference data.

^b Observed at Earth.

^c Flux corrected for $N_{\text{H}} = 1.8 \times 10^{18} \text{ cm}^{-2}$ (Linsky et al. 1993), with H/He abundance ratio set to 11.6.

^d O VIII λ 102.36, 102.49 (H α); Ne VIII λ 103.09; Ni XXIII λ 103.23; Ni XXII λ 103.31. The Fe XIX peak is well isolated. The flux from O VIII H α is not expected to contribute significantly to the Fe XXI flux.

^e Includes Fe XII λ 192.39, Ca XVII λ 192.86, and O V λ 192.8, 192.9. Flux given is the integral of the blue half up to the peak, which agrees well with deblending.

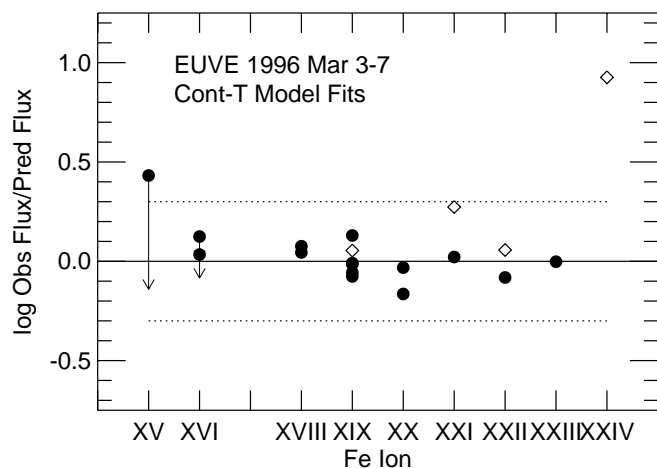


FIG. 4a

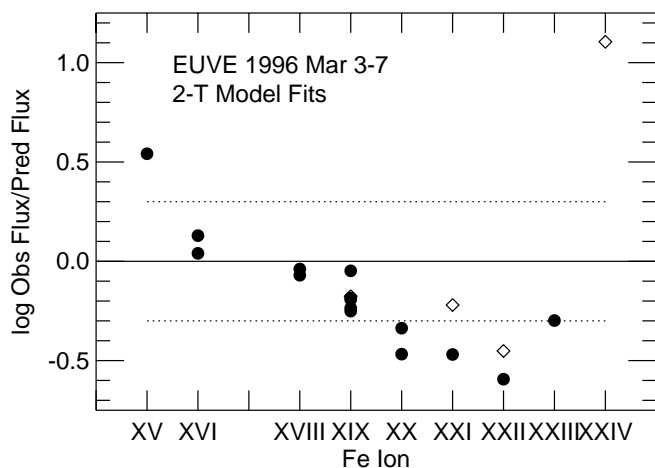


FIG. 4b

FIG. 4.—Observed-to-predicted EUVE line ratios for the models shown in Fig. 3. Filled circles indicate strong unblended lines; diamonds indicate strong but blended lines, as determined either from model predictions or from the observed profile. Note that Fe XVII does not emit strong lines in the EUVE spectral range. Between the dotted lines agreement is within a factor of 2. (a) Comparison for the Cont-T model. For most emission lines the agreement is quite good. The arrows show the effect of including the model below $\log T_e = 6.6$. (b) Comparison for the 2-T EM distribution model, using the VMEKAL-Mod plasma emission model (see the seventh column of Table 2), derived from ASCA. Data have not been adjusted for different normalization between the EUVE and ASCA data. Although the model clearly does not fit many of the EUVE lines, nevertheless, the good agreement of the ASCA model with the strong EUV lines of Fe XVIII confirms the assumption of a common emitting region for the dominant EUV and X-ray emission.

TABLE 2
TWO-TEMPERATURE MODELS FOR CAPELLA^a

| Parameters | Observation Detectors Plasma Model | ASCA 1993 ^e | | ASCA 1996 ^d | | ASCA 1996 ^e | | ASCA 1996 ^f | | ASCA 1996 ^g | |
|------------------------------------|--|------------------------|----------------------|---------------------------|------------------------|------------------------|------------------------|------------------------|------------------------|-------------------------------|--|
| | | 2-T SSS MEKA | 2-T SIS0 VMEKAL | 2-T SIS0 + SIS1 VMEKAL | 2-T SIS0 VMEKAL-Mod | 2-T SIS0 + SIS1 VMEKAL-Mod | |
| $\log [T_1 \text{ (K)}]$ | | 6.68 (6.64, 6.71) | 6.80 (6.75, 6.83) | 6.71 (6.70, 6.73) | 6.81 (6.80, 6.82) | 6.70 (6.61, 6.71) | 6.80 (6.79, 6.81) | 6.70 (6.61, 6.71) | 6.80 (6.79, 6.81) | 6.80 (6.79, 6.81) | |
| $\log [EM_1 \text{ (cm}^3)]$ | | 52.86 (52.74, 52.98) | 53.07 (52.97, 53.15) | 52.80 (52.77, 52.84) | 52.76 (52.73, 52.80) | 52.68 (52.61, 52.77) | 52.75 (52.72, 52.77) | 52.68 (52.61, 52.77) | 52.75 (52.72, 52.77) | 52.75 (52.72, 52.77) | |
| $\log [T_2 \text{ (K)}]$ | | 6.92 (6.89, 6.96) | 7.01 (6.96, 7.03) | 6.92 (6.91, 6.94) | 7.03 (7.00, 7.05) | 6.93 (6.90, 6.96) | 7.02 (6.99, 7.03) | 6.93 (6.90, 6.96) | 7.02 (6.99, 7.03) | 7.02 (6.99, 7.03) | |
| $\log [EM_2 \text{ (cm}^3)]$ | | 52.83 (52.71, 52.94) | 52.74 (52.55, 52.93) | 52.71 (52.65, 52.76) | 52.23 (52.18, 52.32) | 52.58 (52.46, 52.71) | 52.27 (52.23, 52.36) | 52.58 (52.46, 52.71) | 52.27 (52.23, 52.36) | 52.27 (52.23, 52.36) | |
| χ^2_{red} | | 1.27 | 5.51 | 3.15 | 1.00 | 1.20 | 1.21 | 1.20 | 1.21 | 1.21 | |
| dof | | 80 | 63 | 188 | 91 | 87 | 188 | 87 | 188 | 188 | |

^a 90% confidence limits (lower, upper) are given in parentheses.

^b Drake et al. 1994.

^c Models using standard VMEKAL plasma emission code as implemented in XSPEC Version 10.0 for Capella SIS0 detector. Observations of 2 September 1993 PV phase are reduced to 74 PHA channels. Exposure time was 14.4 ks. Derived abundances are given in Table 3. Data and model fit are shown in Fig. 1.

^d Models using standard VMEKAL plasma emission code as implemented in XSPEC Version 10.0 for Capella SIS0 and SIS1 observations of 3 March 1996. Reduced data includes 198 PHA channels. Exposure times were 21.1 and 20.8 ks, respectively. Derived abundances are given in Table 3. Data and model fit are shown in Fig. 5.

^e Models using improved plasma emission model VMEKAL-Mod and calibration adjustments, as described in text, for 1996 SIS0. Derived abundances are given in Table 3. Linear gain fit parameters (slope and offset) are 0.9964 and -0.00115 .

^f Same as footnote e, for 1996 SIS1. Linear gain fit parameters are 0.9868 and 0.0199.

^g Same as footnote e, for 1996 SIS0 + SIS1. Linear gain fit parameters are 0.9932 and 0.00770. Data and model fit are shown in Fig. 9.

TABLE 3
ELEMENTAL ABUNDANCES^a FOR CAPELLA DERIVED FROM TWO-TEMPERATURE MODELS

| Element | Observation Detectors Plasma Model | <i>Einstein</i> 2-T SSS MEKA | <i>ASCA</i> 1993 2-T SIS0 VMEKAL | <i>ASCA</i> 1996 2-T SIS0 + SIS1 VMEKAL | <i>ASCA</i> 1996 2-T SIS0 VMEKAL-Mod | <i>ASCA</i> 1996 2-T SIS1 VMEKAL-Mod | <i>ASCA</i> 1996 2-T SIS0 + SIS1 VMEKAL-Mod |
|----------|--|------------------------------------|--|---|--|--|---|
| N | | 0.00 (0.00, 0.77) | ... | ... | ... | ... | ... |
| O | | 0.13 (0.03, 0.27) | 0.24 (0.16, 0.34) | ... | ... | ... | ... |
| Ne | | 0.15 (0.00, 0.38) | 0.00 (0.00, 0.15) | 0.00 (0.00, 0.05) | 0.00 (0.00, 0.15) | 0.00 (0.00, 0.05) | 0.00 (0.00, 0.12) |
| Mg | | 1.02 (0.80, 1.32) | 0.37 (0.28, 0.48) | 0.96 (0.85, 1.09) | 1.41 (1.23, 1.61) | 0.96 (0.85, 1.09) | 1.40 (1.27, 1.55) |
| Si | | 0.85 (0.67, 1.07) | 0.39 (0.30, 0.49) | 0.81 (0.71, 0.92) | 1.08 (0.93, 1.23) | 0.81 (0.71, 0.92) | 1.12 (1.01, 1.24) |
| S | | 0.73 (0.39, 1.14) | 0.01 (0.00, 0.18) | 0.65 (0.46, 0.85) | 0.92 (0.70, 1.16) | 0.65 (0.46, 0.85) | 0.81 (0.63, 0.99) |
| Fe | | 0.46 (0.36, 0.61) | 0.32 (0.28, 0.37) | 0.54 (0.49, 0.60) | 0.90 (0.81, 0.99) | 0.54 (0.49, 0.60) | 0.90 (0.84, 0.97) |
| Ni | | ... | 0.17 (0.00, 0.49) | 0.49 (0.21, 0.78) | 0.00 (0.00, 0.08) | 0.49 (0.21, 0.78) | 0.00 (0.00, 0.10) |

^a Abundances are given relative to Anders & Grevesse (1989) solar system abundances. Models are given in Table 1; 90% confidence limits (lower, upper) are given in parentheses.

from *Einstein* SSS data (Drake et al. 1994) is reasonably consistent with the 2-T *ASCA* models. While the fit is somewhat better than obtained for the 1993 *ASCA* spectrum, large residuals appear for similar spectral regions. Comparison of the September 1993 and March 1996 spectra (Figs. 1 and 5) shows degradation of the SIS FWHM caused by radiation damage by about one-third, from FWHM = 75 eV to FWHM = 100 eV at 1 keV.

3. INTERDEPENDENCE OF EM DISTRIBUTION AND ABUNDANCE DETERMINATIONS FOR CAPELLA

How much of a poor *ASCA* fit might be attributed to the oversimplification of the EM distribution by a 2-T model? Singh, White, & Drake (1996) address this issue in detail for the RS CVn AR Lac by comparing abundance determinations from 2-T and continuous EM distribution fits to the *ASCA* spectrum. They find that abundance determinations are robust with respect to the EM distribution models derived from *ASCA* data, despite having insufficient spectral resolution to differentiate among models. Since the dominant temperature of the Capella corona is significantly lower than that of AR Lac, with different ions contributing the strong emission lines, we need to test whether the results of Singh et al. (1996) extrapolate to Capella. The result on this issue is summarized in § 6.3.4.

Another important and related issue is the compatibility of spectral models determined from separate fits to the *EUVE* and *ASCA* data. Figure 4b shows the poor agreement of EUV line intensities with the *ASCA* 2-T model predictions. The 2-T model does an acceptable job of predicting the dominant EUV Fe xviii and xix lines but is unacceptable for many other lines. The failure of the *ASCA* model to reproduce the EUV lines of Fe xv and xvi is not surprising, since these ions do not emit in the *ASCA* band. The failure of the model for other lines, from ions which emit in both the *EUVE* and *ASCA* bands, is attributable to the sampling of the large temperature range Fe EUV ionization states. In general, 2-T models will not be able to fit all the Fe EUV lines—the temperature grid needs to be sampled more finely to produce all the ionization states. The shape of the EM distribution, the quality of *EUVE* observations, and the analysis approach for stellar spectra other than those of Capella determine to what extent a 2-T model might be acceptable.

While Singh et al. (1996) limited their exploration of continuous models to simply parameterized models (power-law and polynomial), the simultaneous *ASCA* and *EUVE* spectra allow us to explore more complex EM distribution functions with a small number of variable parameters. Straight application of the *EUVE*-derived models does not

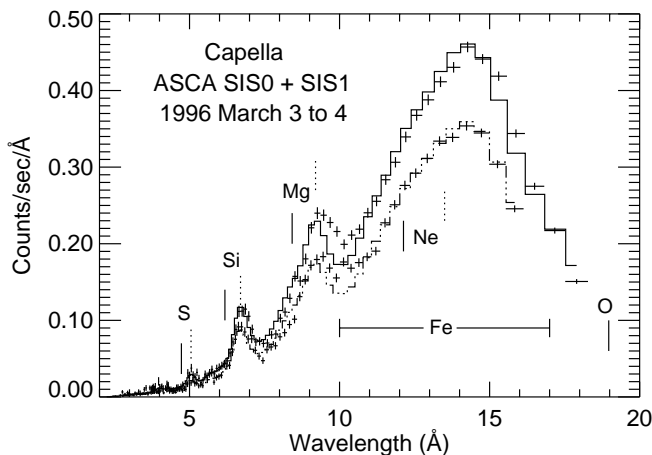


FIG. 5a

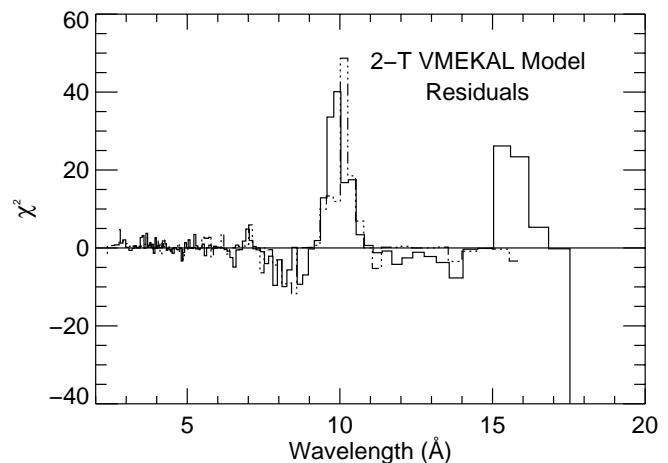


FIG. 5b

FIG. 5.—(a) *ASCA* SIS0 and SIS1 spectra (plus signs) of Capella obtained 1996 March 3–4, with “best” fit ($\chi^2_{\text{red}} = 3.15$) 2-T model (solid line for SIS0; dash-dotted line for SIS1) with variable abundances (model parameters given in Tables 2 and 3). The VMEKAL model in XSPEC is used. Strong line groups are marked, as in Fig. 1. (b) χ^2 with residual sign for each bin, as in Fig. 1.

produce an acceptable *ASCA* model, even after allowing for normalization and abundance adjustments. Nevertheless, the fit is acceptable at the peak of the X-ray spectrum (where X-ray Fe XVIII and XIX lines are emitted), providing confidence in the basic underlying assumptions (see § 4).

4. MODEL UNCERTAINTIES AND IMPROVEMENTS

The SIS spectra are of such high S/N (73,006 net counts with SIS0 and 53,820 net counts with SIS1) that the failure of standard plasma spectral models to fit them should be viewed as an opportunity to examine a number of model inadequacies. The most obvious problem in fitting the *ASCA* spectra is that for all models considered the predicted flux at 10 Å (1.2 keV) is too low. In this section we enumerate the model errors we have considered and describe our efforts to improve the models where possible. In § 5, we return to the question of the structure and abundances of Capella.

4.1. Calibration

The relative calibration uncertainty of a SIS spectrum is believed to be good to $\leq 3\%$ in the range from 0.8 to 6.0 keV (15.5–2.1 Å; see Dotani et al. 1996). The magnitude of the problem between 10 and 12 Å is much larger than that, about 30% to 50%. Furthermore, neither of the possibly problematic energies is affected by edges in the telescope/detector system materials. Both SIS detectors show the same effect. The GIS detectors do not show this, but since their energy resolution and effective areas at these energies are lower, any effects probably would be washed out.

The SIS gain offsets do not appear to be consistent with each other below 0.8 keV (a problem possibly caused by radiation/cosmic ray damage). This offset problem occurs with the new spectra and does not seem to occur with the PV phase spectra. We ignore all SIS1 channels with energy below 0.8 keV (> 15.5 Å) and all SIS0 channels with energy below 0.7 keV (> 17.7 Å). Allowing the gain offsets to vary for each SIS spectrum separately does not in itself resolve the fitting problem using standard plasma spectral models. As we discuss below, once spectral models approach an acceptable fit, gain calibration errors become noticeable around the line complexes of Mg (~ 9.2 Å) and Si (~ 6.6 Å), and thus we will allow for gain calibration corrections in our final models.

4.2. Uncertainties in Atomic Rates and the Prediction of Emission-Line Intensities

4.2.1. Fe Ionization Balance

The Fe ionization balance of Arnaud & Raymond (1992) has rather large uncertainties. Brickhouse et al. (1995) have undertaken a systematic analysis of the atomic data uncertainties of the EUV Fe lines, showing that different ionization balance models could lead to large uncertainties in the shape of EM distributions. Capella, with its EM distribution enhancement around 6×10^6 K, is particularly sensitive to the large differences in the predicted dielectronic recombination rates from Fe XVII (see Fig. 4 in Brickhouse et al.). Masai (1997) discusses similar effects of ionization balance on temperatures and Fe abundances derived from *ASCA* for temperatures in the 0.4–1.0 keV range.

To test the sensitivity of the fit to the Fe ionization balance, we compute separate models for each Fe ion using the table model option in XSPEC (Arnaud 1996) and the

SPEX (Kaastra, Mewe, & Nieuwenhuijzen 1996) line-emissivity table. We then allow the relative Fe ion “abundances” to vary. Within limits based on fairly large uncertainty estimates, we do not find a fit much better than the original fits. Left to its own devices, the XSPEC algorithm eliminates the Fe XX to XXII ions altogether in order to remove unwanted flux at 12 Å (1.0 keV); however, *EUVE* spectra demonstrate that these ions exist. We conclude that the Fe ionization balance uncertainty cannot by itself account for the modeling problem.

4.2.2. Fe L-Shell Ion ($n = 4 \rightarrow 2$)/($n = 3 \rightarrow 2$) Line Ratios

Liedahl, Osterheld, & Goldstein (1995) have computed the Fe L-shell ion $n = 4 \rightarrow 2$ and $n = 3 \rightarrow 2$ line emissivities, which are incorporated in the MEKAL and SPEX models. For Fe XXIV, the computed line ratios agree with recent laboratory experiments (Savin et al. 1996). Other laboratory measurements are underway. It is difficult to design a simple test within XSPEC for these line ratios in the Capella spectrum. On the other hand, there is no obvious line or group of lines in the problem wavebands for which the atomic data are uncertain enough to improve the fit substantially.

4.2.3. Ni Ionization Balance

The MEKAL model incorporates the ionization balance model of Arnaud & Rothenflug (1985), except for Fe, for which the model of Arnaud & Raymond (1992) is used. Differences in dielectronic recombination rate coefficients between the two models for Fe of up to factors of 4 are significant in shifting the temperature dependences of the relative ion populations. The ionization balance for Ni should be corrected to be consistent with Arnaud & Raymond (1992). We have scaled the Ni ion populations from the Fe models using the ratio of the square of the nuclear charge for each isosequence and include this modification in our improved model, VMEKAL-Mod (see § 4.3). Figure 6 shows that the differences are noteworthy; however, this change does not lead to a noticeable improvement in the fit to the Capella data.

4.3. Incompleteness of the Atomic Models and the Effects of “Missing Lines”

The *ASCA* Capella fitting problem led us to reevaluate the completeness of the plasma emission models. D. A. Liedahl & N. S. Brickhouse (1999, in preparation) show that lines originating from energy levels with high principal quantum numbers ($n > 5$) may contribute significant flux to specific energy bands. Such high-energy lines of the Fe L-shell ions contribute to the spectrum around 10 Å.

VMEKAL models include lines up to $n = 5$ for the Fe L-shell ions. New calculations using the Hebrew University/Lawrence Livermore Atomic Code (HULLAC) (Klapisch 1971; Klapisch et al. 1977; Liedahl, Osterheld, & Goldstein 1995) generate emissivity tables for $n = 6, 7$, and $8 \rightarrow 2$ transitions for Fe XVII, $n = 6$, and $7 \rightarrow 2$ for Fe XVIII, and $n = 6 \rightarrow 2$ for Fe XIX. These calculations are in good agreement with recent Livermore electron beam ion trap (EBIT) measurements for Fe XVII (Brown et al. 1998). Brown et al. detect and identify Fe XVII lines up to $n = 11 \rightarrow 2$. Figure 7 compares the affected spectral region with and without these additional lines for a model with single temperature $T_e = 6 \times 10^6$ K, showing that the high excitation lines of Fe XVII–XIX increase the flux in the 1 Å

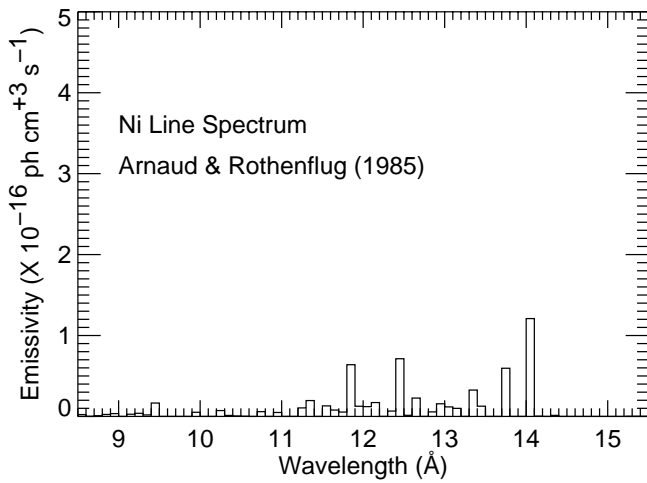


FIG. 6a

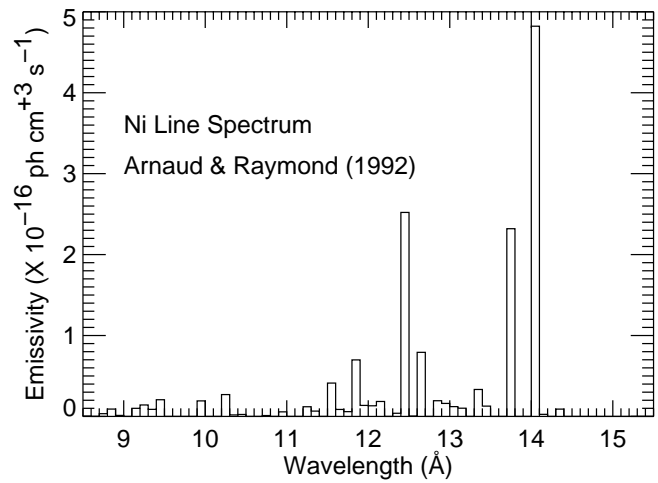


FIG. 6b

FIG. 6.—(a) Ni emission spectrum computed with the SPEX code, assuming the Arnaud & Rothenflug (1985) ionization balance. This model is essentially the model used in the XSPEC MEKAL model. (b) Ni emission spectrum computed with our improved ionization balance models, as described in the text.

interval centered at 10.3 \AA by 74%. We include these lines in our improved model VMEKAL-Mod (see next section).

5. STRUCTURE AND ABUNDANCES OF CAPELLA WITH IMPROVED MODELS

We report both 2-T and *EUVE*-derived EM distribution model fits using a spectral model we will call VMEKAL-Mod. The VMEKAL-Mod model is a modification of the VMEKAL model in XSPEC version 10.0 with additive user-defined XSPEC table models (see Arnaud 1996) for Fe and Ni. We set the Ni abundance to zero and add Ni table models that incorporate an ionization balance scaled from the Fe models of Arnaud & Raymond (1992). Fe table models are added to the Fe model in VMEKAL to incorporate the additional lines of high n from D. A. Liedahl & N. S. Brickhouse (1999, in preparation).

We derive “best-fit” models for SIS0 and SIS1 independently and for the two detectors together (Tables 2, 3, and 4). Since the SIS0 spectrum has more counts, the joint fits are naturally weighted toward SIS0. Abundances for ele-

ments not listed are fixed at the AG89 value, with the exception of O. The O abundance has been allowed to vary in order to improve the fit; however, the O abundances derived are neither robust nor statistically significant and we do not report them.

Differences between the two detectors near the O line ($\lambda 18.97$) suggest a calibration problem, as noted. The gain corrections found for the SIS0 and SIS1 bear out the different calibrations, but the sensitivity to the O abundance makes the gain correction unreliable as well. We have ensured that the gain corrections derived through the spectral fitting process improve the spectral line complexes near Si and Mg, but otherwise these corrections are better viewed as adjustable factors to allow for systematic uncertainties on the order of a few percent. Figure 8 shows the effects of the gain correction for the 2-T VMEKAL-Mod plasma emission model. In particular, the model Si line around 6.7 \AA becomes centered when the gain is corrected. As discussed above, gain corrections alone do not provide improved fits, and only with the improved atomic plus EM

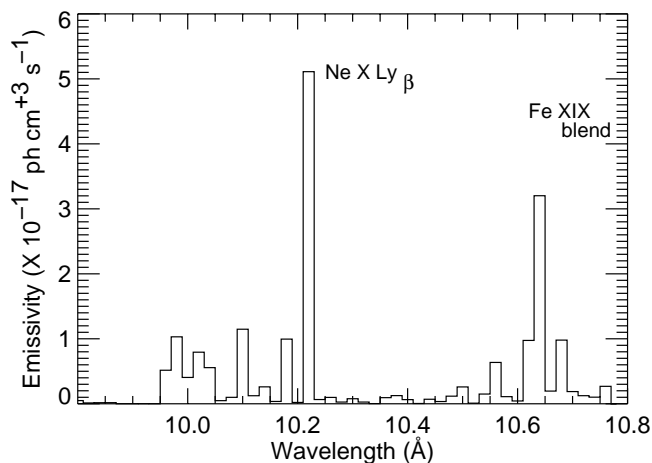


FIG. 7a

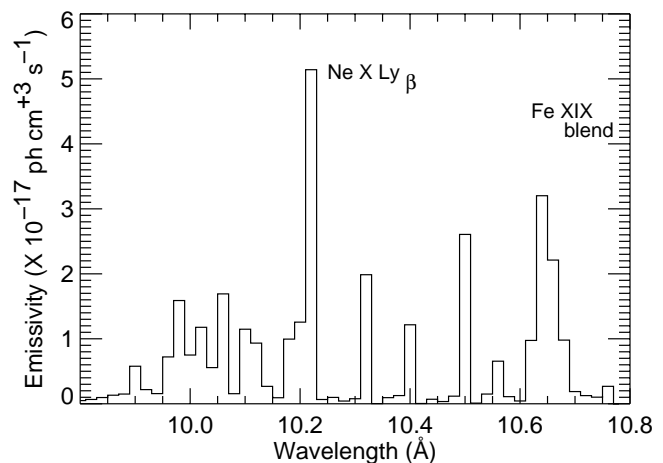


FIG. 7b

FIG. 7.—Emission model of SPEX for the spectral region around 10 \AA (a) compared with the same model, plus the additional lines for high n excitations of D. A. Liedahl & N. S. Brickhouse (1999, in preparation). (b) currently missing in plasma spectral codes. The model shown is for $\log T_e = 6.8$, the peak of the Capella EM distribution. The bin size used for this display is 0.02 \AA .

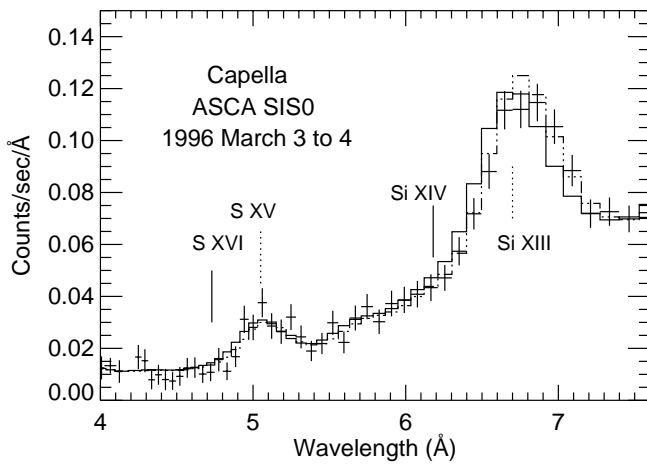


FIG. 8a

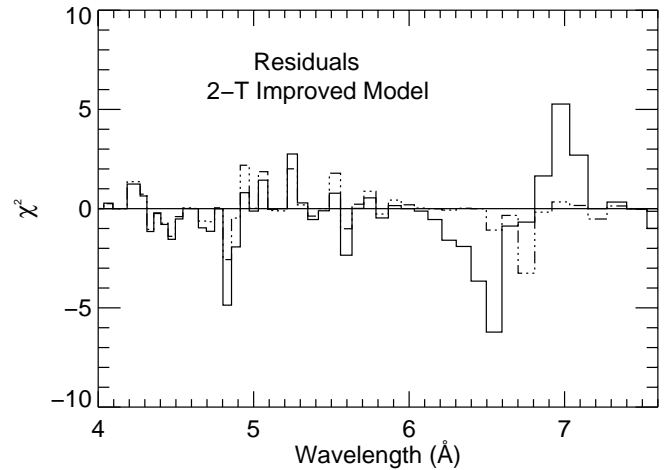


FIG. 8b

FIG. 8.—(a) Region of the *ASCA* SIS0 spectrum of Capella showing the effects of allowing a gain correction for the 2-T VMEKAL-Mod plasma emission model. The dash-dotted curve is the model with the gain correction derived from the fit, while the solid curve shows the same model with no gain adjustment. The H-like Ly α line positions of Si and S are labeled and marked with solid lines, while the strongest He-like lines are marked with dotted lines. (b) χ^2 with residual sign for each bin, as in Fig. 1. Both models are shown. Note in particular the offset of the computed peak of the Si line around 6.7 Å from the observed peak.

distribution models are we able to establish the importance of correcting the gain.

5.1. Results Using the VMEKAL-Mod Model

The parameters of the “best-fit” 2-T models with improved VMEKAL-Mod plasma model are listed in Tables 2 and 3. Comparison of the data and fit is shown in Figure 9.

For the *EUVE*-derived models using VMEKAL-Mod, we fix the shape of the EM distribution as shown in Figure 3, allowing only a single overall normalization factor for the emission measures to adjust for calibration effects between *EUVE* and *ASCA*. (We note again that the EM distribution in Fig. 3 has already been adjusted to obtain the correct high-energy cut-off of the *ASCA* spectrum.) The “best-fit”

model parameters are given in the sixth column of Table 4, with the comparison of the data and fit shown in Figure 10. The normalization factor needed to convert the *EUVE*-derived EM distribution to the *ASCA* best-fit model is 1.21, well within the expected limits.

Small fit residuals near the 10 Å band indicate that problems with models remain. Experimental verification of the theoretical calculation of the high n line strengths is provided by Brown et al. (1998) for Fe xvii, with good agreement. Some mismatch between the EUV and X-ray models might also be expected from either excitation rate or ionization balance inaccuracies. We have not determined the cause of the poor fit between 15 and 17 Å of the SIS0 spectrum, and it is disturbing that SIS0 and SIS1 do not agree. It is possible that the optical brightness of Capella affects the SIS CCD gain (see Dotani et al. 1996).

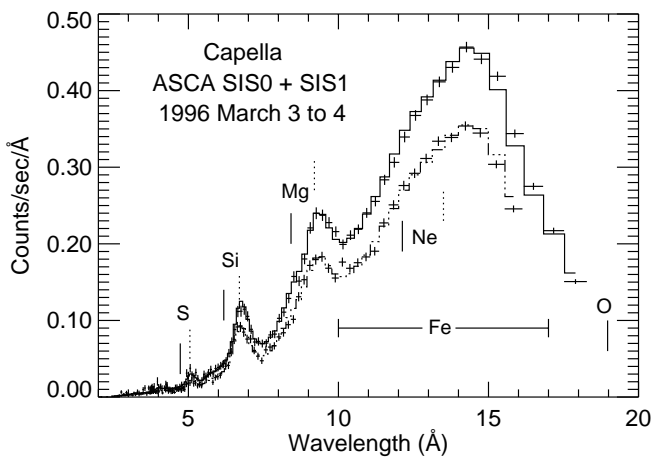


FIG. 9a

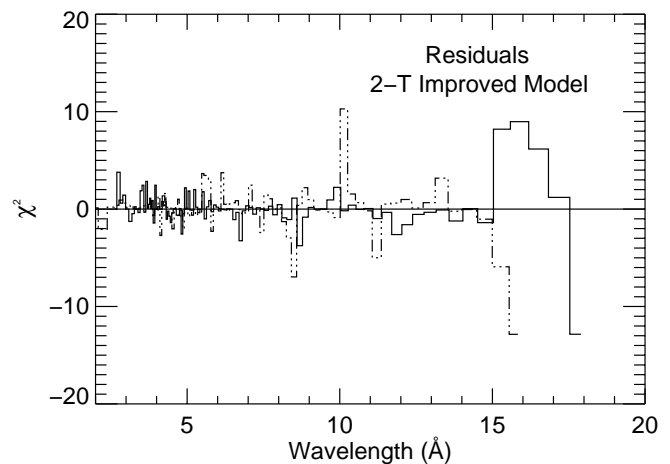


FIG. 9b

FIG. 9.—(a) *ASCA* SIS0 and SIS1 spectra of Capella obtained 1996 March 3–4, with best fit ($\chi^2_{\text{red}} = 1.21$) 2-T model with variable abundances (model shown in Fig. 3 as crosses, with parameters given in Tables 2 and 3). The VMEKAL model in XSPEC has been modified, as described in the text. While this model provides a good fit to the *ASCA* spectra, it does not fit the *EUVE* spectrum (see Fig. 4). Strong line groups are marked, as in Fig. 1. (b) χ^2 with residual sign for each bin, as in Fig. 1.

TABLE 4
ELEMENTAL ABUNDANCES^a FOR CAPELLA DERIVED FROM CONTINUOUS-TEMPERATURE (CONT-T) MODELS

| Parameters | Observation | <i>EUVE</i> ^b | <i>EUVE</i> Lines | <i>ASCA/EUVE</i> 1996 ^c | <i>ASCA/EUVE</i> 1996 ^d | <i>ASCA/EUVE</i> 1996 ^e |
|---|--------------|--------------------------|---------------------------|------------------------------------|------------------------------------|------------------------------------|
| | Detectors | Cont-T | | Cont-T SIS0 | Cont-T SIS1 | Cont-T SIS0 + SIS1 |
| | Plasma Model | | | VMEKAL-Mod | VMEKAL-Mod | VMEKAL-Mod |
| O | | 0.42 ± 0.18 | O VIII λ102.45 | ... | ... | ... |
| Ne | | ... | ... | 0.37 (0.14, 0.55) | 0.03 (0.00, 0.26) | 0.26 (0.07, 0.42) |
| Mg | | ... | ... | 1.18 (0.98, 1.36) | 1.03 (0.90, 1.23) | 1.34 (1.17, 1.49) |
| Si | | 1.99 ± 0.38 | Si XII λλ499.40, 520.67 | 1.06 (0.92, 1.18) | 1.17 (1.03, 1.31) | 1.30 (1.20, 1.41) |
| S | | 1.15 ± 0.18 | S XIV λλ417.61, 445.77 | 0.97 (0.71, 1.22) | 0.74 (0.47, 1.01) | 1.10 (0.90, 1.32) |
| Ar | | 2.41 ± 0.31 | Ar XVI λλ353.92, 389.14 | ... | ... | ... |
| Fe | | 0.88 ± 0.13 ^f | (all) | 0.65 (0.57, 0.72) | 0.58 (0.54, 0.66) | 0.72 (0.66, 0.78) |
| Ni | | 1.81 ± 0.20 | Ni XVII λ249.18 | 0.13 (0.00, 0.30) | 0.70 (0.53, 0.82) | 0.38 (0.25, 0.53) |
| | | | Ni XVIII λλ291.97, 320.54 | ... | ... | ... |
| log [<i>EM</i> _{peak} (cm ³)] | | 52.60 | N/A | 52.85 (52.81, 52.89) | 52.82 (52.78, 52.84) | 52.77 (52.74, 52.80) |
| χ^2_{red} | | N/A | N/A | 1.68 | 1.33 | 1.87 |
| dof | | N/A | N/A | 94 | 90 | 191 |

^a Abundances are given relative to Anders & Grevesse (1989) solar system abundances. Error limits for *EUVE* data are given as $\pm 1 \sigma$, while 90% confidence limits (lower, upper) for *ASCA*-derived parameters are given in parentheses.

^b Results are from Brickhouse (1996). The Fe/H abundance ratio is determined by measuring the “apparent” continuum level, making it a lower limit, with the largest errors coming from the continuum measurement. The shape of the EM distribution is determined from Fe lines only. Abundances other than Fe are determined from the observed lines listed in the next column, with 1σ errors derived from the statistical significance of the line intensities.

^c This work, with EM distribution shape fixed from *EUVE* Fe line intensities and peak adjusted from fitting. Abundances not given are fixed to the solar value, except for O; O abundance is allowed to vary but is not considered to be reliable. Gain fit corrections are the same as given in Table 1.

^d Same as footnote c, for SIS1. Gain fit corrections are the same as given in Table 1.

^e Same as footnote c, for SIS0 + SIS1. Gain fit parameters are 0.9850 and 0.0152. EM distribution model is shown in Fig. 3. Data and model fit are shown in Fig. 10.

^f The value of 0.88 is properly interpreted as a lower limit, since the ratio of the true to apparent continuum is not known. Brickhouse (1996) estimates that the weak line contribution is less than $\sim 10\%$.

The modifications to the model clearly affect not only the goodness-of-fit statistic, but also the derived abundances. Table 3 illustrates that for the 2-T models, the increase in derived abundances for Mg, Si, S, and Fe from the 1996 *ASCA* SIS0 + SIS1 spectra ranges from 25% to 67%, with more modest (but significant) differences in temperatures and emission measures. Similar increases in abundances occur for the Cont-T model (not listed in Table 4).

Using the modified plasma models, abundances derived from both SIS spectra for Mg, Si, and S are in substantial agreement from the 2-T and Cont-T EM distribution models; however, the derived Fe abundance is actually sig-

nificantly lower in the Cont-T case. The Fe abundance is closely coupled in the inverse sense to the continuum emission through the normalization (*EM*) parameter. Furthermore, the abundances of Ni and Ne show wide differences in the various cases. The derived Ni abundances do not appear to be reliable; Ne appears to be generally low relative to its AG89 value by a factor of about 3 or more.

While one might naively expect the parameters derived from SIS0 + SIS1 spectra together to be some weighted average of the values derived from the individual SIS spectra, the models are not well enough constrained for this expectation to be met. For the 2-T models, the derived

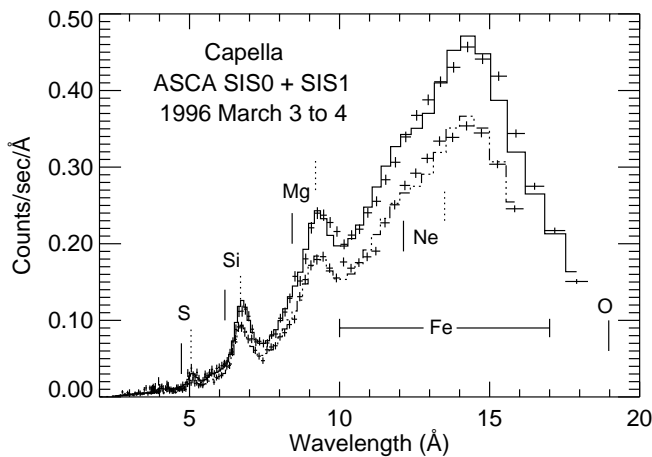


FIG. 10a

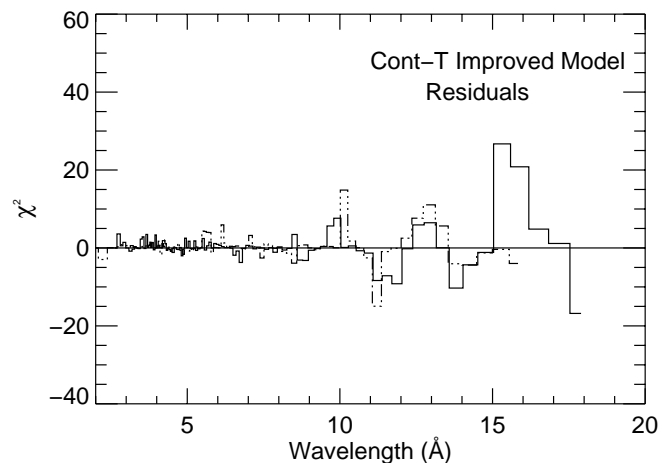


FIG. 10b

FIG. 10.—(a) *ASCA* SIS0 and SIS1 spectra of Capella obtained 1996 March 3–4, with best fit ($\chi^2_{\text{red}} = 1.87$) Cont-T EM distribution model with variable abundances. This provides a good fit to the *EUVE* observations shown in Fig. 3. Its parameters are given in Table 4. The VMEKAL model in XSPEC has been modified, as described in the text. Strong line groups are marked, as in Fig. 1. (b) χ^2 with residual sign for each bin, as in Fig. 1.

parameters from SIS0 + SIS1 seem pegged to the SIS0 values, presumably because the SIS0 spectrum has more counts. Of interest, as Table 4 shows, for the Cont-T models, both of the individual SIS fits produce lower abundances (and thus higher EM normalizations) than the joint fit (the shape of the EM distribution having remained fixed). The complex blend of lines and continuum in the intrinsic spectrum, complicated by expected uncertainties in the models and calibration, only provide constraints on the abundances at about the 50% level. On the other hand, the Cont-T models from SIS0, SIS1, and SIS0 + SIS1 are in substantially better agreement with each other than for the 2-T models. For the 2-T models, the SIS0 and SIS1 best-fit parameters are clearly in disagreement with each other.

Table 5 gives our adopted abundances for the Capella corona and compares them with solar photospheric and coronal values. The preferred values are taken from the Cont-T model using SIS0 + SIS1. Confidence intervals are expanded to include best-fit values from SIS0 and SIS1 independently where necessary. The confidence interval has also been expanded for Fe to include the *EUVE* result of Brickhouse (1996), discussed in § 6.3.2.

6. DISCUSSION

Using the best-fit Cont-T model for Capella, we investigate the working assumptions implicit in determining the structure and abundances. We also consider consistency checks for isolated *ASCA* features. Finally, this section addresses the generality of these results for other *ASCA* analyses.

6.1. Source Physics

6.1.1. Equilibrium Ionization

When the charge-state distribution is not fully equilibrated with the local electron temperature, line ratios based on collisional ionization equilibrium are not accurate. For Fe L-shell ions that are ionizing, one would expect the observed $n = 3 \rightarrow 2/n = 2 \rightarrow 2$ ratio to be higher than the equilibrium prediction, just as observations of a somewhat overionized plasma would give values lower than the equilibrium prediction. (As the plasma becomes more strongly overionized, recombination cascades begin to dominate over collisional excitation as the level population mechanism, grossly changing the spectrum.) Since many of the dominant ions in the *EUVE* spectrum ($n = 2 \rightarrow 2$ lines of Fe XVIII–XXIV) also emit lines in the *ASCA* band around

1 keV ($n = 3 \rightarrow 2$ and $n = 4 \rightarrow 2$ lines of the same Fe L-shell ions), the good agreement of the peak of the *ASCA* count spectrum (predominantly Fe XVII to XIX line emission) is notable (see Fig. 4b). Thus the assumption of ionization equilibrium remains justified for now.

6.1.2. Optical Depth

The possibility that strong resonance line photons are scattered out of the line of sight (see Schrijver et al. 1995) cannot be ruled out entirely by the existing empirical evidence. Brickhouse et al. (1995) show that the strong EUV resonance line intensities in Capella Fe XVIII $\lambda 93.94$ and Fe XIX $\lambda 108.37$ are in excellent agreement with the intensities of other lines sharing the same upper levels, Fe XVIII $\lambda 103.94$ and Fe XIX $\lambda 120.00$, respectively. Predictions based on branching ratios thus rule out resonance scattering in the EUV as an explanation for inferring a low line-to-continuum ratio.

Even without individual line-intensity observations of X-ray resonance and nonresonance lines, we can estimate the extent to which optical depth effects might play a role in reducing the observed X-ray line-to-continuum ratios. For Doppler broadened lines, the optical depth τ as parameterized by Mewe et al. (1994) is:

$$\tau = 1.16 \times 10^{-14} \frac{n_{\text{ion}}}{n_{\text{el}}} A_z \frac{N_{\text{H}}}{N_e} \lambda f \sqrt{\frac{M}{T_e}} \int N_e dl, \quad (1)$$

where $n_{\text{ion}}/n_{\text{el}}$ is the fraction of the element population in ionization state ion, A_z is the element abundance relative to H, $N_{\text{H}}/N_e = 0.85$ for a fully ionized plasma with cosmic abundance, λ is the wavelength in Å, f is the oscillator strength, M is the atomic weight, and T_e is the electron temperature in K.

Using this approximation, we assume AG89 abundances, the ionization balance of MEKAL-Mod, and a single-temperature model characterized by the peak of the EM distribution at 6×10^6 K. This single-temperature model is justified for this estimate because all of the lines to be discussed are dominated by this temperature when one folds their emissivity curves through the EM distribution. The line in the high-temperature spectrum with the largest value of τ is Fe XVII $\lambda 115.01$. The value of τ for $\lambda 115.01$ is constrained by the observed ratio of line intensities of Fe XVIII resonance line $\lambda 93.92$ and Fe XVIII $\lambda 103.94$, emitted from the same upper level. The observed branching ratio of 2.92 from Table 1 is in excellent agreement with the predicted ratio of

TABLE 5
ELEMENTAL ABUNDANCES^a FOR CAPELLA

| ELEMENT | CAPELLA ^b | SOLAR PHOTOSPHERE | | SOLAR CORONA | |
|----------|------------------------------------|------------------------|-----------------------|-----------------------|-----------------------|
| | This Work | Anders & Grevesse 1989 | Grevesse et al. 1992 | Meyer 1985 | Feldman et al. 1992 |
| O | ... | 8.51×10^{-4} | 7.41×10^{-4} | 2.47×10^{-4} | 7.76×10^{-4} |
| Ne | 3.20×10^{-5} (0.37, 5.17) | 1.23×10^{-4} | 1.20×10^{-4} | 3.53×10^{-5} | 1.20×10^{-4} |
| Mg | 5.09×10^{-5} (3.91, 5.67) | 3.80×10^{-5} | ... | 3.73×10^{-5} | 1.41×10^{-4} |
| Si | 4.62×10^{-5} (3.76, 5.01) | 3.55×10^{-5} | ... | 3.92×10^{-5} | 1.26×10^{-4} |
| S | 1.78×10^{-5} (1.20, 2.14) | 1.62×10^{-5} | ... | 8.63×10^{-6} | 1.86×10^{-5} |
| Ar | ... | 3.63×10^{-6} | 3.31×10^{-6} | 2.12×10^{-6} | 3.80×10^{-6} |
| Fe | 3.37×10^{-5} (2.71, 4.41) | 4.68×10^{-5} | 3.25×10^{-5} | 3.92×10^{-5} | 1.26×10^{-4} |
| Ni | ... | 1.78×10^{-6} | ... | 2.16×10^{-6} | 6.92×10^{-6} |

^a Abundances are given relative to the H abundance.

^b Confidence limits ([lower, upper] times the exponential), as described in the text, are given in parentheses.

2.71 (Brickhouse et al. 1995). Systematic uncertainties in the theoretical transition probabilities and line blending dominate over the statistical errors. We estimate the uncertainty to be less than 25%, ruling out a larger reduction in the $\lambda 93.92$ line intensity; hence $\tau \leq 0.3$ in $\lambda 93.92$. Constraints imposed on other strong X-ray resonance lines are Fe xvii $\lambda 15.01$ ($\tau \leq 3.6$); O viii Ly α $\lambda 18.97$ ($\tau \leq 0.7$); Fe xviii $\lambda 14.20$ ($\tau \leq 0.7$), and Ne x Ly α $\lambda 12.14$ ($\tau \leq 0.5$). O viii Ly α has been resolved and measured in Capella with the *Einstein* FPCS (Vedder & Canizares 1983), and its flux is also in reasonable agreement (to better than a factor of 2) with the *EUVE*-derived EM distribution, AG89 abundances, and $\tau = 0$, quite consistent with the limit from the EUV lines.

With these upper limits on optical depth in lines, one obtains $\int N_e dl \leq 10^{20} \text{ cm}^{-2}$. Density-sensitive line ratios observed with *EUVE* give $N_e \sim 10^{12} \text{ cm}^{-3}$ (Dupree et al. 1993; Brickhouse 1996), suggesting that the depth of the effective emitting region is $\leq 10^8 \text{ cm}$ ($\leq .001 R_\star$). Even if one were to argue that the line ratios are not good density diagnostics (see Griffiths & Jordan 1998) and conservatively took a solar coronal active region density of 10^9 cm^{-3} , the corresponding effective emitting region depth would still be less than the stellar radius. The emission measure places an additional constraint on the emitting volume for a given density that is consistent with the hot emitting volume being smaller, most likely much smaller, than that of the star. As Dupree et al. (1993) have pointed out, coronal magnetic fields of order several hundred gauss are required to support the smaller, higher density regions.

Brickhouse et al. (1997) considered the possibility that the intensity ratio of Ne x Ly α $\lambda 12.13$ to Ly β $\lambda 10.24$ is reduced by optical depth effects as an explanation for the *ASCA* fitting problem. The addition of high excitation Fe lines eliminates the need for measurable optical depth in $\lambda 12.13$ and allows good agreement of the Ne x Ly α to Ly β ratio with theoretical calculations. Since optical depth effects, if present, are small, we retain the assumption of negligible optical depth.

6.2. Emission-Measure Distribution

The failure of 2-T models to reproduce the *EUVE* line intensities clearly indicates their inadequacy for high-resolution spectral analysis. On the other hand, values of χ_{red}^2 from fits to the *ASCA* spectra using the Cont-T models are not as good as those from the 2-T fits to the *ASCA* spectra alone. Since the shape of the EMD model is fixed entirely by the *EUVE* data, systematic uncertainties in atomic data (e.g., ionization balance, collision strengths) are likely to be contributing to the problems. As suggested above, Fe xvii $\lambda 15.01$ may exhibit some optical depth effects as well. The χ_{red}^2 is consistent with systematic uncertainties discussed throughout this paper. The use of a purely statistical figure of merit is not justified for such high S/N data, whereas the overall consistency of the model with both data sets lends credibility to our results. Thus we adopt the abundances listed in Table 5 using the more realistic EM distribution.

The persisting failure of any model, including Cont-T EM distribution VMEKAL-Mod models, to fit the 1993 Performance Verification (PV) *ASCA* spectrum suggests that other improvements to the models are needed, although it is difficult to determine what the problems are. As noted, the earlier SIS spectra are of higher spectral resolution and thus may be more sensitive to model errors.

6.3. Abundances

6.3.1. Abundances from Other X-Ray Observations

The coronal abundances we report here are generally higher than have been reported from previous analyses of X-ray observations. Models of the *ROSAT* PSPC observations indicate that the overall abundance level is 0.2 times solar (Bauer & Bregman 1996); however, the calibration of the low-energy *ROSAT* response appears to be significantly in error, accounting for some of the discrepancy between these results and ours (Napiwotzki et al. 1993; Brickhouse & Dupree 1998). Schrijver et al. (1995) find that reducing the Fe abundance reduces the need for a very high energy EM distribution tail (now shown to be unreal with our simultaneous *EUVE* and *ASCA* spectra) to fit *EUVE* spectra. At least part of the explanation for their low EUV line-to-continuum ratio is their choice of ionization balance model, which has since been revised (J. Kaastra 1996, private communication). Analysis of the recent SAX observation of Capella indicates a best-fit coronal metallicity of 0.68 ± 0.05 times the AG89 value, consistent with our values (Favata et al. 1997).

6.3.2. Abundances from EUVE

The Fe/H abundance ratio reported here is in good agreement with previous *EUVE* results, which are listed in Table 4 (Brickhouse 1996). The EUV determination is based on the summed spectrum from five pointings (for a total of 280 ks), thus providing high enough S/N to measure directly the “apparent” continuum throughout the SW waveband. Since the “apparent” continuum contains an unknown contribution from unresolved, weak line emission, the actual continuum emission is less than the measured value. Hence, the Brickhouse (1996) Fe/H abundance ratio is properly interpreted as a lower limit. Thus, the good agreement of the *ASCA* derivation with the previous *EUVE* results suggests that missing lines in the models of the EUV spectrum may not make a significant contribution to the pseudo-continuum for a source as hot as Capella; missing lines are likely to be more important for a lower temperature source such as Procyon (see Schmitt, Drake, & Stern 1996; Beiersdorfer et al. 1999).

Brickhouse (1996) also reports elemental abundance measurements from the Li-like doublet lines of Si and S in the *EUVE* Long Wavelength (LW) spectrometer that are in reasonable agreement with the *ASCA* abundances determined primarily from the He-like ion complexes at 6.6 Å (Si) and 5.1 Å (S).

6.3.3. The Ne Abundance

The Ne abundance is consistently low for all *ASCA* models. Figure 11 shows that assuming a solar Ne abundance gives a strong signature of Ne ix and x emission lines, and thus we rule out such a high Ne abundance. The rather large spread in Ne (and Ni) abundances that we derive using different models results from the inextricable blending of Ne, Ni, and Fe at the resolution of *ASCA*. Our best estimate of the Ne abundance, accounting for systematic uncertainties, puts it lower than solar by a factor of about 3 to 4.

The Anders & Grevesse (1989) value for the solar photospheric abundance of Ne is derived from both solar and local galactic data, which are in good agreement with each other. Our results for the Fe to Ne ratio, while suggestive of a First Ionization Potential (FIP) effect, need to be verified for other high FIP elements, as well as with respect to

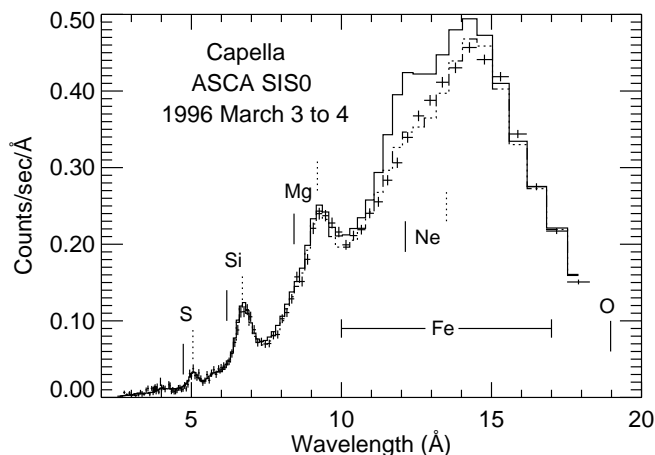


FIG. 11a

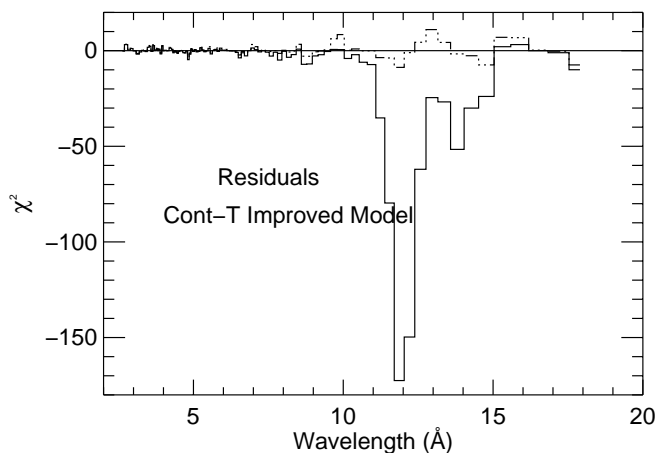


FIG. 11b

FIG. 11.—(a) *ASCA* SIS0 spectrum of Capella showing the fit of the Cont-T model of Table 4 (dash-dotted line) with low Ne abundance compared with the same model for the Anders & Grevesse (1989) Ne abundance (solid line). Strong line groups are marked, as in Fig. 1. (b) χ^2 with residual sign for each bin, as in Fig. 1. Both models are shown.

photospheric abundances of Capella. We note that if a FIP effect interpretation is indicated, the sense is that high FIP species are depleted with respect to H, consistent with Phillips et al. (1994) for a solar flare and Raymond et al. (1997) for a coronal streamer, but opposite to the findings of Feldman (1992).

6.3.4. Comparison of Abundances Derived from Different Models

The EM distribution bump dominates the spectrum much like a single temperature. Thus the robustness of the abundances derived primarily from isolated features formed at this temperature is not surprising.

We illustrate the model-dependence of abundance determinations by considering a Line-Based Approach (LBA) to the Si abundance. Since the He-like Si line complex is strong and well isolated, the Si abundance determined from *ASCA* depends only on the EM distribution model and the continuum subtraction from the line complex. If we assume the EM distribution model from *EUVE*, then upper and lower limits on the Si line emission are easily determined by imposing a Gaussian line profile at the He-like Si feature. The continuum emission to be subtracted from the feature must be between zero and the maximum level determined by visual inspection. Our adopted model prediction gives a value roughly in the middle of these two limits. Hence, with an independently determined model and visual inspection of the relevant spectral region, we determine the Si abundance to about $\pm 30\%$. While the errors are larger than the statistical errors found from either the 2-T or Cont-T models, the results do not depend on a global fit to the *ASCA* spectrum.

6.4. How General Are the Capella Results for *ASCA* Spectral Analysis?

Caution is required in extrapolating these results to other *ASCA* spectra. A few comments are in order. (1) Including the high n lines in the spectral model significantly increases the derived heavy-element abundances by decreasing the continuum emission in the models. (2) The systematic uncertainties are clearly larger than the statistical errors. Without clear guidance as to how to treat the instrumental effects, the conservative choice is to use both SIS detectors in the analysis. (3) These analyses provide no evidence that

the *ASCA* calibration is worse than expected: the gain corrections are small, and the low-energy response is consistent with radiation damage, such that SIS0 and SIS1 appear to have roughly 10% disagreement as to the effective area at ~ 0.8 keV. (4) The Capella spectrum is sufficiently soft so that line-free spectral bins do not exist within the SIS bandpass and spectral resolution. The ability to identify line-free spectral bins in other *ASCA* spectra might enable better constraints to be placed on models for hotter sources. (5) The “best-fit” EM distribution model (i.e., the 2-T model) to *ASCA* alone is clearly ruled out by *EUVE* observations. Abundances of the four most prominent elements are, nevertheless, fairly well determined using the 2-T model, in this case because one of the two temperatures in the 2-T model agrees well with the prominent EM distribution “bump” identified by *EUVE*. In the absence of *EUVE* spectra, the robustness of abundance derivations with respect to models needs to be tested on a case-by-case basis. (6) The abundances of Mg, Si, and S, which have relatively isolated lines in the SIS spectra, are robust at about the 30% level with respect to the 2-T and Cont-T EM distribution models. The Ne abundance is more sensitive to the models, but there is general agreement that it is lower than solar (AG89) by at least a factor of 3. For Fe, 2-T and Cont-T abundances do not formally agree.

7. CONCLUSIONS

We demonstrate a good degree of consistency between *ASCA* and *EUVE* for the temperature structure and abundances of the Capella binary system. The dominance of an EM distribution bump around 6×10^6 K and the lack of a hot EM distribution “tail” (cf. Schrijver et al. 1995) are confirmed by these observations. Our results indicate that Mg, Si, S, and Fe have solar abundances (i.e., Anders & Grevesse 1989) to within 50%, while Ne is subsolar by a factor of at least 3 to 4. *Chandra* and *XMM* observations of Capella should confirm these basic results while establishing whether the composite coronal abundance pattern is a true FIP effect by providing measurements of high FIP elements.

We have demonstrated that the new Fe calculations of D. A. Liedahl & N. S. Brickhouse (1999, in preparation)

provide a marked improvement in the fit of plasma spectral models to the *ASCA* Capella spectrum. Model flux deficits around 1.2–1.4 keV are apparent for other *ASCA* sources as well: numerous cool stars (e.g., β Ceti, Drake et al. 1994), the elliptical galaxy M87 (Hwang et al. 1997), and the composite supernova remnant MSH 11-62 (Harrus, Hughes, & Slane 1997). More work remains to be done to assess the significance of other “missing lines” in the X-ray range.

CCD-resolution detectors will continue to be important for studies of extended sources with the next generation of X-ray missions. Thus, benchmarking the plasma codes with the high S/N grating observations of *Chandra* and *XMM*,

coupled with *EUVE* spectra for stellar coronal sources such as Capella, will provide invaluable input to the process of improving the models. Our results also indicate the need for laboratory experiments to assess the accuracy of the plasma spectral models.

This work was supported in part by NAG 5-3422, NAG 5-3389, NAG 5-3559, NAS 8-40224, and NAS 8-39073 from NASA to the Smithsonian Astrophysical Observatory. Work at the Lawrence Livermore National Laboratory was performed under the auspices of the U. S. Department of Energy, Contract No. W-7405-Eng-48.

REFERENCES

- Anders, E., & Grevesse, N. 1989, *Geochim. Cosmochim. Acta*, 53, 197 (AG89)
- Antunes, A., Nagase, F., & White, N. E. 1994, *ApJ*, 436, L83
- Arnaud, K. A. 1996, in *ASP Conf. Ser. 101, Astronomical Data Analysis Systems V*, ed. G. Jacoby & J. Barnes (San Francisco: ASP), 17
- Arnaud, M., & Raymond, J. C. 1992, *ApJ*, 398, 394
- Arnaud, M., & Rothenflug, R. 1985, *A&AS*, 60, 425
- Ayres, T. R. 1988, *ApJ*, 331, 467
- Ayres, T. R., Simon, T., Stern, R. A., Drake, S. A., Wood, B. E., & Brown, A. 1998, *ApJ*, 496, 428
- Ayres, T. R., Schiffer, F. H., & Linsky, J. L. 1983, *ApJ*, 272, 223
- Ayres, T. R., et al. 1995, *ApJS*, 96, 223
- Bauer, F., & Bregman, J. N. 1996, *ApJ*, 457, 382
- Beiersdorfer, P., Lepson, J. K., Brown, G. V., Utter, S. B., Kahn, S. M., Liedahl, D. A., & Mauche, C. W. 1999, *ApJ*, 519, L185
- Brickhouse, N. S. 1996, in *IAU Colloq. 152, Astrophysics in the Extreme Ultraviolet*, ed. S. Bowyer & R. F. Malina (Dordrecht: Kluwer), 105
- Brickhouse, N. S., & Dupree, A. K. 1998, *ApJ*, 502, 918
- Brickhouse, N. S., Dupree, A. K., & Raymond, J. C. 1996, in *ASP Conf. Ser. 109, Cool Stars, Stellar Systems, and the Sun, Ninth Cambridge Workshop*, ed. R. Pallavicini & A. K. Dupree (San Francisco: ASP), 253
- Brickhouse, N. S., Dupree, A. K., Edgar, R. J., Drake, S. A., White, N. E., Liedahl, D. A., & Singh, K. P. 1997, *BAAS*, 29, 808
- Brickhouse, N. S., Raymond, J. C., & Smith, B. W. 1995, *ApJS*, 97, 551
- Brown, G. V., Beiersdorfer, P., Liedahl, D. A., Widmann, K., & Kahn, S. M. 1988, *ApJ*, 502, 1015
- Catura, R. C., Acton, L. W., & Johnson, H. M. 1975, *ApJ*, 196, L47
- Dotani, T., et al. 1996, *ASCA Newsl.*, No. 4, 3
- Drake, J. J., Laming, J. M., & Widing, K. G. 1995, *ApJ*, 443, 393
- , 1997, *ApJ*, 478, 403
- Drake, S. A. 1996, in *ASP Conf. Ser. 99, Cosmic Abundances*, ed. S. S. Holt & G. Sonneborn (San Francisco: ASP), 215
- Drake, S. A., Singh, K. P., & White, N. E. 1996, in *ASP Conf. Ser. 109, Cool Stars, Stellar Systems, and the Sun, Ninth Cambridge Workshop*, ed. R. Pallavicini & A. K. Dupree (San Francisco: ASP), 263
- Drake, S. A., Singh, K. P., White, N. E., & Simon, T. 1994, *ApJ*, 436, L87
- Dupree, A. K. 1996, in *ASP Conf. Ser. 109, Cool Stars, Stellar Systems, and the Sun, Ninth Cambridge Workshop*, ed. R. Pallavicini & A. K. Dupree (San Francisco: ASP), 237
- Dupree, A. K., & Brickhouse, N. S. 1996, in *Poster Proc., IAU Symp. 176: Stellar Surface Structure* (Wien: Institut für Astronomie), 184
- Dupree, A. K., Brickhouse, N. S., Doschek, G. A., Green, J. C., & Raymond, J. C. 1993, *ApJ*, 418, L41
- Eggen, O. J. 1960, *MNRAS*, 120, 540
- Favata, F., Mewe, R., Brickhouse, N. S., Pallavicini, R., Micela, G., & Dupree, A. K. 1997, *A&A*, 324, L37
- Feldman, U. 1992, *Phys. Scr.*, 46, 202
- Feldman, U., Mandelbaum, P., Seely, J. F., Doschek, G. A., & Gursky, H. 1992, *ApJS*, 81, 387
- Grevesse, N., Noels, A., & Sauval, A. J. 1992, in *Proc. First SOHO Workshop: Coronal Streamers, Coronal Loops, and Coronal and Solar Wind Composition* (Brussels: ESA), 305
- Griffiths, N. E., & Jordan, C. 1998, *ApJ*, 497, 883
- Harrus, I. M., Hughes, J. P., & Slane, P. O. 1997, *ApJ*, 499, 273
- Holt, S. S., White, N. E., Becker, R. H., Boldt, E. A., Mushotzky, R. F., Serlemitsos, P. J., & Smith, B. W. 1979, *ApJ*, 234, L65
- Hummel, C. A., Armstrong, J. T., Quirrenbach, A., Buscher, D. F., Mozurkewich, D., & Elias, N. M., II. 1994, *AJ*, 107, 1859
- Hwang, U., Mushotzky, R. F., Loewenstein, M., Markert, T. H., Fukazawa, Y., & Matsumoto, H. 1997, *ApJ*, 476, 560
- Jordan, C., Doschek, G. A., Drake, J. J., Galvin, A. B., & Raymond, J. C. 1998, in *ASP Conf. Ser. 154, Cool Stars, Stellar Systems, and the Sun, Tenth Cambridge Workshop*, ed. R. A. Donahue & J. A. Bookbinder (San Francisco: ASP), 91
- Kaastra, J. S., Mewe, R., & Nieuwenhuijzen, H. 1996, in *UV and X-ray Spectroscopy of Astrophysical and Laboratory Plasmas*, ed. K. Yamashita & T. Watanabe (Tokyo: Universal Academy), 411
- Kimble, R. A., et al. 1993, *ApJ*, 404, 663
- Klapisch, M. 1971, *Comput. Phys. Commun.*, 2, 239
- Klapisch, M., Schwab, J. L., Fraenkel, J. S., & Oreg, J. 1977, *J. Opt. Soc. Am.*, 61, 148
- Lemen, J. R., Mewe, R., Schrijver, C. J., & Fludra, A. 1989, *ApJ*, 341, 474
- Liedahl, D. A., Osterheld, A. L., & Goldstein, W. H. 1995, *ApJ*, 438, L115
- Linsky, J. L., et al. 1993, *ApJ*, 402, 694
- Linsky, J. L., Wood, B. E., Brown, A., & Osten, R. A. 1998, *ApJ*, 492, 767
- Masai, K. 1997, *A&A*, 324, 410
- McWilliam, A. 1990, *ApJS*, 74, 1075
- Mewe, R., et al. 1982, *ApJ*, 260, 233
- Mewe, R., Kaastra, J. S., Schrijver, C. J., van den Oord, G. H. J., & Alkemade, F. J. M. 1994, *A&A*, 296, 477
- Mewe, R., Kaastra, J. S., White, S. M., & Pallavicini, R. 1996, *A&A*, 315, 170
- Meyer, J.-P. 1985, *ApJS*, 57, 173
- Naftilan, S. A., & Drake, S. A. 1977, *ApJ*, 216, 508
- Napiwotzki, R., Barstow, M. A., Fleming, T., Holweger, H., Jordan, S., & Werner, K. 1993, *A&A*, 278, 478
- Ortolani, A., Maggio, A., Pallavicini, R., Sciortino, S., Drake, J. J., & Drake, S. A. 1997, *A&A*, 325, 664
- Perryman, M. A. C., et al. 1997, *A&A*, 323, L49
- Phillips, K. J. H., Pike, C. D., Lang, J., Watanabe, T., & Takahashi, M. 1994, *ApJ*, 435, 888
- Pilachowski, C. A., & Sowell, J. R. 1992, *AJ*, 103, 1668
- Randich, S., Giampapa, M. S., & Pallavicini, R. 1994, *A&A*, 283, 893
- Randich, S., Gratton, R., & Pallavicini, R. 1993, *A&A*, 273, 194
- Raymond, J. C., et al. 1997, *Sol. Phys.*, 175, 645
- Savin, D., et al. 1996, *ApJ*, 470, L73
- Schmitt, J. H. M. M., Drake, J. J., & Stern, R. A. 1996, *ApJ*, 465, L51
- Schmitt, J. H. M. M., Stern, R. A., Drake, J. J., & Kuerster, M. 1996, *ApJ*, 464, 898
- Schrijver, C. J., Lemen, J. R., & Mewe, R. 1989, *ApJ*, 341, 484
- Schrijver, C. J., Mewe, R., van den Oord, G. H. J., & Kaastra, J. S. 1995, *A&A*, 302, 438
- Sheeley, N. R. 1996, *ApJ*, 469, 423
- Singh, K. P., White, N. E., & Drake, S. A. 1996, *ApJ*, 456, 766
- Stern, R. A., Lemen, J. R., Schmitt, J. H. M. M., & Pye, J. P. 1995, *ApJ*, 444, L45
- Strassmeier, K. G., & Fekel, F. C. 1990, *A&A*, 230, 389
- Swank, J. H., White, N. E., Holt, S. S., & Becker, R. H. 1981, *ApJ*, 246, 208
- van den Oord, G. H. J., Schrijver, C. J., Camphens, M., Mewe, R., & Kaastra, J. S. 1997, *A&A*, 326, 1090
- Vedder, P. W., & Canizares, C. R. 1983, *ApJ*, 270, 666
- White, N. E., et al. 1994, *PASJ*, 46, L97